

Article

# An Augmented Social Network Search Algorithm for Optimal Reactive Power Dispatch Problem

Shahenda Sarhan <sup>1</sup>, Abdullah Shaheen <sup>2,\*</sup> , Ragab El-Sehiemy <sup>3</sup>  and Mona Gafar <sup>4,5</sup><sup>1</sup> Faculty of Computing and Information Technology, King Abdulaziz University, Jeddah 21589, Saudi Arabia<sup>2</sup> Department of Electrical Engineering, Faculty of Engineering, Suez University, Suez 43533, Egypt<sup>3</sup> Department of Electrical Engineering, Faculty of Engineering, Kafrelsheikh University, Kafrelsheikh 33516, Egypt<sup>4</sup> Department of Computer Science, College of Science and Humanities in Al-Sulail, Prince Sattam bin Abdulaziz University, Kharj 16273, Saudi Arabia<sup>5</sup> Machine Learning and Information Retrieval Department, Artificial Intelligence, Kafrelsheikh University, Kafrelsheikh 33516, Egypt\* Correspondence: [abdullahshaheen2015@gmail.com](mailto:abdullahshaheen2015@gmail.com)

**Abstract:** Optimal Reactive Power Dispatch (ORPD) is one of the main challenges in power system operations. ORPD is a non-linear optimization task that aims to reduce the active power losses in the transmission grid, minimize voltage variations, and improve the system voltage stability. This paper proposes an intelligent augmented social network search (ASNS) algorithm for meeting the previous aims compared with the social network search (SNS) algorithm. The social network users' dialogue, imitation, creativity, and disputation moods drive the core of the SNS algorithm. The proposed ASNS enhances SNS performance by boosting the search capability surrounding the best possible solution, with the goal of improving its globally searched possibilities while attempting to avoid getting locked in a locally optimal one. The performance of ASNS is evaluated compared with SNS on three IEEE standard grids, IEEE 30-, 57-, and 118-bus test systems, for enhanced results. Diverse comparisons and statistical analyses are applied to validate the performance. Results indicated that ASNS supports the diversity of populations in addition to achieving superiority in reducing power losses up to 22% and improving voltage profiles up to 90.3% for the tested power grids.



**Citation:** Sarhan, S.; Shaheen, A.; El-Sehiemy, R.; Gafar, M. An Augmented Social Network Search Algorithm for Optimal Reactive Power Dispatch Problem.

*Mathematics* **2023**, *11*, 1236. <https://doi.org/10.3390/math11051236>

Academic Editor: Mario Versaci

Received: 28 January 2023

Revised: 25 February 2023

Accepted: 27 February 2023

Published: 3 March 2023



**Copyright:** © 2023 by the authors. Licensee MDPI, Basel, Switzerland. This article is an open access article distributed under the terms and conditions of the Creative Commons Attribution (CC BY) license (<https://creativecommons.org/licenses/by/4.0/>).

**Keywords:** social network search; effective exploitation strategy; electrical power grids; optimal reactive power dispatch; voltage profile; power losses

**MSC:** 68T20

## 1. Introduction

### 1.1. Motivation

With the recent massive increase in the cost of petroleum fuel and its direct and indirect impact on people's daily lives, focus has shifted to optimizing active and reactive power flow in order to improve the economics and security of power system operations. Furthermore, increasing power consumption is critical for assisting the electrical power industry in planning and ensuring the appropriate operation of electrical power infrastructure [1,2]. Optimal Power Flow (OPF) is a non-convex, non-continuous, non-linear, large-scale, and constrained optimization problem through which control variables are optimized while satisfying both equality and inequality constraints.

The process of reaching parameter values that minimize the overall function is called optimization. Most search algorithms suffer from local minimum where the algorithm manages to find the minimal value within the nearby points but perhaps fails to reach the minimal value in all other possible places in the problem state space. The key point is to find global optima. Global optimization is a major issue that faces search algorithms.

The key motivation of this research is to reach a global optima in the ORPD problem work space [3].

ORPD is one of the challenges of OPF and one of the most important responsibilities in the power system network operation [3,4]. The primary goal of the ORPD is to reduce real power losses and voltage variations while improving system voltage stability, considering several equality and inequality constraints, including voltages of generators, power flows through the lines, voltages of load buses, reactive power production, and transformer taps. Furthermore, ORPD aims to determine the best-operating settings of the control variables, such as transformer tap, generator voltage, and the number of compensation devices to be switched [5].

### 1.2. Literature Review

In recent years, a range of novel and meta-heuristic optimization techniques have been effectively presented for solving engineering problems. They are becoming increasingly prominent in several academic fields for tackling difficult optimization problems. These stochastic techniques are applied in several aspects of power system optimization. An improved chaotic harmony search optimizer has been introduced, integrating the chaotic patterns for generating random numbers with uniform distribution to solve the dispatch problem while combining environmental and economic objectives [6]. In [7], a biogeography-based optimizer (BBO) has been used for OPF issues with valve point non-linearities, but it has only been evaluated for small IEEE 9-bus and 30-bus systems. In [8], a modified version of the Slime-Mould algorithm (SMA) has been applied to solve the economic-emission dispatch problem, with updated equations from the sine-cosine technique included to increase the SMA's performance. In addition, a moth flame algorithm has been utilized for the unit commitment problem in order to find the optimal scheduling of the generation units [9]. Furthermore, an artificial gorilla algorithm has been developed for solving the multi-dimensional optimal power flow problem [10], while a genetic algorithm combining a time series has been presented to search for the optimal allocation of reactive power compensation devices considering the impacts of distributed generators [11].

Over the past few years, many optimizers have been introduced to tackle the ORPD issues. Conventional optimization approaches such as linear programming [12], the Newton method [13], quadratic programming [14], and the interior-point method [15] were the most widely employed optimizers in the early years. In [16], a fuzzy-based procedure (FLP) approach was used to maximize the impact of preventive control activities related to reactive power to overcome any emergency circumstance that arose. FLP was used in this work to reduce violation limitations and provide an appropriate reactive power reserve for multi-operating scenarios. However, these approaches frequently have drawbacks, such as converging to the nearest optimum, incapability of dealing with non-linear and non-convex limitations, discontinuity forms of objective functions, and situations with many local minimum locations. As a result, new strategies for overcoming these limitations have to be developed.

Evolutionary computing optimizers have been used for solving the ORPD as QEA [17], PSO [18], hybrid PSO [19], BFA [20], adaptive real-coded GA [21], CLPSO [22], harmony search algorithm [23], GSA [24], DE algorithm [25], hybrid PSO and ICA [26], and exchange market algorithm [27].

Recently, a novel improved ALO algorithm [28,29], GB-WCA [30], multi-objective ALO algorithm [31], hybrid swarm intelligence [32], enhanced teaching learning-based optimization algorithm [33], ILAO [34], tunicate swarm algorithm [35], and AEO [36] have been employed to solve the ORPD with consideration of different constraints. In [37], an improved variant of the evaporation rate water cycle algorithm (ERWCA) has been presented to regulate the directional overcurrent relays in power systems. In this study, an oppositional learning strategy with Levy-flight was incorporated into ERWCA to prevent landing on the local optimum and increase the convergence rate, and it was validated on

the CEC'2017 test suite and compared to other algorithms. In [38], a beetle antenna search algorithm was implemented to address the optimal active power dispatch in addition to enhancing the electrical performance of power networks by reducing fuel expenditure, air pollution, and power losses.

In The hybrid multi-swarm PSO algorithm was demonstrated in [25] to overcome the problem of OPRD while increasing the voltage profile and reducing real power loss. In [39], the EFA has been utilized to solve the ORPD and optimally active problems. In [40], the MODE has been characterized as solving the OPRD by reducing the power loss, the voltage deviation, and increasing the voltage stability. In [41], the convex quadratic optimization program has been elaborated to sustain the voltage bus even in the unbalanced distribution system. In [42], QODE has been successfully applied to solve the ORPD problem by reducing the power loss, improving the voltage profile, and increasing the voltage stability.

While in [43], FA has been combined with the APT-FPSO and applied to the ORPD problem with IEEE 30-bus, IEEE 57-bus, and IEEE 118-bus, considering the voltage stability index and voltage magnitude deviations. In [44], the ABC algorithm has been applied on ORPD IEEE 30- and 57-bus grids with consideration of voltage stability enhancement, real power loss minimization, and voltage deviation minimization. In [45], SHADE has been applied to ORPD IEEE 30-bus and 57-bus with steady-state voltage deviation and real power loss. To address the reactive power flow issue in power systems, accelerated bio-inspired optimization (ABO) was used [46]. Despite the fact that the results were significant, the obtained operating points in this study required feasibility validations.

In [47], a SCA was being used to handle the ORPD issue more efficiently than other meta-heuristic techniques. However, because this was a single objective minimization work, only power losses were considered. In [48], a WOA has been utilized to solve the ORPD task with applications on the IEEE 14-bus, IEEE 30-bus, and practical Algerian electrical network. In this study, the performance of WOA showed efficient performance compared to PSO and PSO-TVAC. However, the reported comparisons were only performed as a single objective optimization for network losses. In [49], a SBDE algorithm has been presented to handle the ORPD issue and achieve the maximum reduction of grid losses. However, the performance assessment of the presented SBDE algorithm compared with the GA was only applied to small grids of IEEE 14- and IEEE 30-bus grids.

In 2022, different studies have been proposed to solve ORPD issues, as in [50], an IMPA is introduced. IMPA improved the marine predator algorithm exploration and exploitation techniques by updating the predator position to be near the best predator using spiral movement. The IMPA was only tested using the IEEE 30-bus system and showed superiority over the original MPA. In [51], the CTFWO algorithm was introduced. The CTFWO algorithm enhances the exploration rate of the conventional TFWO using chaotic maps. The CTFWO was tested on two bus systems, the IEEE 30-bus and IEEE 57-bus. In [52], the authors introduced the CAC-DE hybrid approach, through which the best compromise solution is found using Fuzzy Logic. CAC-DE has effectively reduced the power loss, but it has not performed the same for the Voltage Stability Index. Furthermore, the authors proposed new algorithms in radial distribution networks for reducing energy loss and capacitor investment in order to reduce costs [53]. They proposed a hybridization of evolutionary algorithms with a sensitivity-based decision-making technique for the optimal planning of shunt capacitors [54] and a novel combined evolutionary algorithm for the optimal planning of distributed generators [55]. Finally, ref. [56] finds optimal solutions for the placement of reactive and active power generation components in distribution networks using a high-performance meta-heuristic algorithm.

### 1.3. Research Gap

The SNS algorithm was driven by social networking participants in various moods such as imitation, discussion, disputation, and creativity in attitudes used to express people's new ideas on current events [57]. To begin, an imitation mood is created in which people must evaluate the viewpoints of other individuals in order to copy other users in

expressing their particular opinions. Secondly, the dialogue mood is simulated, in which people may link and share the perspectives of others. Thirdly, the disputation mood is simulated, in which people can debate their opinions with a group of other users. Fourthly, the creativity mood is simulated, in which people analyze a topic that is generally related to their fresh convictions. According to [58], the SNS algorithm was used for OPF in its traditional configuration, but its related reliability required additional supports and adaptations in the fields of power simulations and optimizations, mathematical benchmarking frameworks, and complex engineering challenges. As a result, in this article, an ASNS algorithm for multi-dimensional ORPD in power grids is presented. Two enhancements are incorporated to improve the performance of the SNS algorithm. In the beginning, an effective exploitation strategy is intended to increase the seeking of the best view by all users. Second, because exploiting support is necessary towards the end of iterations, an adjustable variable is provided for this procedure. As this value grows, so does the level of support for the exploiting feature provided by the offered effective strategy [59].

#### 1.4. Problem Statement

ORPD is one of the most important responsibilities in power system network operations. It targets determining the best-operating settings of the control variables, such as transformer tap, generator voltage, and the number of compensation devices to be switched. The primary goal of the ORPD is to reduce real power losses and voltage variations while improving system voltage stability. Several equality and inequality constraints must be handled, including voltages of generators, power flows through the lines, voltages of load buses, reactive power production, and transformer taps.

#### 1.5. Major Contributions of this Study and Paper Organization

The following are the major contributions described in this work:

- A novel ASNS algorithm with an effective exploitation strategy is introduced.
- A novel ASNS algorithm-inspired scheme for handling the ORPD problem is offered and scrutinized on three typical IEEE test grids of different sizes.
- A test is executed to authenticate the statistical efficacy of the suggested ASNS-inspired scheme.
- The suggested ASNS algorithm presents a robust and straightforward solution for the ORPD problem under two-goal functions of minimizing grid losses and voltage deviations.
- The simulation results disclose the dominance of the suggested ASNS algorithm over many solvers that were recently reported in the literature.

The following portions of this work are organized as follows: Section 2 presents the design framework for the ORPD optimization problem. Section 3 also establishes the basic SNS and the suggested ASNS, whereas Section 4 defines the discussions and simulation findings. Finally, Section 5 concludes this paper.

## 2. ORPD Formulation

In the ORPD issue, the decision variables are the generator voltages that are denoted by  $(VG_1, VG_2, \dots, VG_{NG})$ , the transformer tap settings that are denoted by  $(Ta_1, Ta_2, \dots, Ta_{NT})$ , and the reactive power (VAr) supplied by switched capacitors and reactors, which are denoted by  $(Qr_1, Qr_2, \dots, Qr_{Nr})$ , respectively. The values NG, Nr, and NT indicate the number of generators, the number of VAr sources, and the number of on-load tap transformers. The dependent variables include load bus voltage magnitudes, VAr outputs of the generators, and transmission line loadings, which are demonstrated by  $(VL_1, \dots, VL_{NPQ})$ ,  $(QG_1, QG_2, \dots, QG_{NG})$ , and  $(SF_1, \dots, SF_{NL})$ , respectively. The values NPQ and NL indicate the number of load buses and the number of transmission lines. As a result, the ORPD problem may be mathematically stated as shown in the following equation:

$$\text{Min } F_n = \{f_1(X_u, X_v), f_2(X_u, X_v)\} \text{ Subjected to : } M(X_u, X_v) = 0 \text{ and } N(X_u, X_v) \leq 0 \quad (1)$$

### 2.1. Problem Objectives

The primary goal of the ORPD issue is to reduce two technical objectives: real power losses in the transmission grid and voltage variations across the buses. Therefore, both technical objectives are investigated as follows:

#### 2.1.1. Total Grid Losses

The minimization of TGLs in MW can be computed as [60]:

$$TGLs = \sum_{i=1}^{Nb} \sum_{j=1}^{Nb} G_{ij}(V_i^2 + V_j^2 - 2(V_i V_j \cos \theta_{ij})) \tag{2}$$

#### 2.1.2. Voltage Profile Improvement

The voltage profile gets improved by reducing the total voltage deviation (TVD) for the buses by 1 p.u. as follows:

$$VD = \sum_{i=1}^{Nb} |V_i - V_{ref}| \tag{3}$$

#### 2.1.3. Voltage Stability Improvement

This objective function is introduced in order to improve voltage stability by decreasing the maximum voltage stability index (L-index), which is used in [61]. The L-index for each bus  $j$  ( $L_j$ ) is established as follows:

$$L_j = \left| 1 - \sum_{i=1}^{N_g} F_{ji} \frac{V_i}{V_j} \angle(\theta_{ij} + \delta_i - \delta_j) \right| \tag{4}$$

$$F_{ji} = [Y_{LL}]^{-1} [Y_{LG}] \tag{5}$$

To increase the system's VSI, the maximum L-index should be reduced as follows:

$$VSI = \text{Max} (L_j)_{j = 1, 2, \dots, N_b} \tag{6}$$

### 2.2. Problem Constraints

#### 2.2.1. The Inequality Constraints

The power system has to satisfy different inequality constraints corresponding to the operational variables. For the decision variables, Equations (7)–(9) describe the inequality constraints of the generator voltages, the transformer tap settings, and the reactive power injected into switched capacitors and reactors, respectively [62].

$$VG_k^{min} \leq VG_k \leq VG_k^{max}, k = 1 : NG \tag{7}$$

$$Ta_l^{min} \leq Ta_l \leq Ta_l^{max}, l = 1 : NT \tag{8}$$

$$Qr_s^{max} \leq Qr_s \leq Qr_s^{max}, s = 1 : Nr \tag{9}$$

For the dependent variables, Equations (10)–(12) describe the inequality constraints of the load bus voltage magnitudes, the reactive power outputs of the generators, and transmission line loadings, respectively:

$$VL_m^{min} \leq VL_m \leq VL_m^{max}, m = 1 : NPQ \tag{10}$$

$$|SF_L| \leq SF_L^{max}, L = 1 : NL \tag{11}$$

$$QG_k^{min} \leq QG_k \leq QG_k^{max}, k = 1 : NG \tag{12}$$

### 2.2.2. The Equality Constraints

These constraints are represented by the load flow balance equations, as denoted in Equations (13) and (14):

$$Pg_i - PL_i - V_i \sum_{j=1}^{Nb} V_j (G_{ij} \cos \theta_{ij} + B_{ij} \sin \theta_{ij}) = 0, \quad i = 1, \dots, Nb \quad (13)$$

$$Qg_i - QL_i + Qr_i - V_i \sum_{j=1}^{Nb} V_j (G_{ij} \sin \theta_{ij} - B_{ij} \cos \theta_{ij}) = 0, \quad i = 1, 2, \dots, Nb \quad (14)$$

where  $Pg_i$  is the output power of each generator (i);  $PL_i$  and  $QL_i$  are the active and reactive power demands of each load (i);  $B_{ij}$  is the mutual susceptance between bus  $i$  and  $j$ , respectively;  $G_{ij}$  is the conductance of every line connecting buses  $i$  and  $j$ ;  $\theta$ ,  $V$ , and  $N_b$  are the phase angle, voltage, and number of buses, respectively; and  $Qg_i$  is the VAR output of each generator (i).

## 3. Proposed ASNS for Solving the ORPD Problem

### 3.1. Basic SNS Algorithm

The SNS framework is derived from participants on social networking sites, where people try to be attractive and express a variety of moods [57]. Such attitudes are techniques for sharing people’s fresh perspectives on a new occurrence. Firstly, the imitation mood is simulated, in which people must consider the perspectives of various individuals to emulate other users in expressing their personal thoughts. Secondly, the dialogue mood is simulated, in which people may link and share the perspectives of others. Thirdly, the disputation mood is simulated, in which people can debate their opinions with a group of other users. Fourthly, the creativity mood is simulated, in which people analyze a topic that is generally related to their fresh convictions. The four inspired moods of the SNS are mathematically described as:

#### 3.1.1. Imitation

If there is a new event with an interesting notion, members can imitate renowned people by attempting to publish a thread that discusses this topic. This state of mind could be expressed as follows:

$$U_{i,new} = U_j + r_1 \times r_2 \times (U_i - U_j) \quad (15)$$

#### 3.1.2. Dialogue

People may learn more about an event by exchanging thoughts with one another from various points of view and then generating a fresh perspective on the event. This state of mind can be expressed numerically as:

$$U_{i,new} = U_k + r_1 \times [\text{sign}(f_i - f_j)(U_i - U_j)] \quad (16)$$

The term  $[\text{sign}(f_i - f_j)(U_i - U_j)]$  illustrates the diversity in the viewpoints of the users.

#### 3.1.3. Disputation

People in this mood can communicate and advocate their viewpoints with remarks or discussions; however, they could be persuaded by other established commentators to exchange ideas about a specific issue. This state of mind can be expressed as:

$$U_{i,new} = U_i + r_1 \times [U_{mean} - ((1 + \text{round}(r_1)) \times U_i)] \quad (17)$$

where the mean vector within a group or commenters’ views of friends is defined in Equation (18):

$$U_{mean} = \frac{1}{N_{group}} \sum_{u=1}^{N_{group}} U_u \quad (18)$$

### 3.1.4. Creativity

Users can express themselves creatively and innovatively regarding a given topic. As a result, a fresh concept will be generated, and this mood can be expressed as:

$$U_{i,new}^d = t_2 U_j^d + (1 - r_2)(r_1 \times (UB^d - LB^d) + LB^d) \tag{19}$$

### 3.1.5. Rules Related to the Network

Each social network defines a set of roles for its users, and these roles are regarded by all users from shared perspectives. The following factors are used to limit the users' perspectives:

$$U_{k,new} = \min(U_{k,new}, UB_k) \& U_{k,new} = \max(U_{k,new}, LB_k), k = 1 : D \tag{20}$$

### 3.1.6. Rules for Publishing

The SNS method is produced by various moods, in which every user's viewpoint is modified and fresh views are adopted based on their merit. To demonstrate, if the new idea is superior to the existing one, it will be approved. As a result, the value of a new idea can be quantitatively estimated by its fitness function as follows:

$$U_i = \begin{cases} U_i & f(U_{i,new}) > f(U_i) \\ U_{i,new} & f(U_{i,new}) < f(U_i) \end{cases} \tag{21}$$

To design SNS, the starting viewpoint for every user may be created as:

$$U_0 = (rand(0,1) \times (UB - LB)) + LB \tag{22}$$

## 3.2. ASNS with an Effective Exploitation Strategy

To increase the performance of the algorithm, an ASNS algorithm with EES is used. The performance of the SNS algorithm is improved with two adjustments. In the beginning, an EES is intended to improve the search capability for of all users. As a result, the basic SNS's upgrading process has been adjusted, and the viewpoints of many users have been altered as follows:

$$U_{i,new}^d = U_{best}^d + t \times r \tag{23}$$

$$r = U_i - U_j \tag{24}$$

$$t = rand(0,1) \tag{25}$$

Second, because exploitation support is required at the end of iterations, an adjustable parameter ( $\alpha$ ) is created using Equation (26) [63,64]:

$$\alpha = \frac{t}{2 * T^{max}} \tag{26}$$

Using this formula, this parameter is grown directly proportional to the number of iterations until it reaches 0.5 of its upper level. The offered EES gives more support for the exploitative feature as this value increases. The suggested EES in Equation (26) is not engaged until more than half of the iterations have been completed, as indicated in [64]. As a consequence of this stance, the ASNS's superior diversifying skills in uncovering newer prospective sectors are retained. Moreover, since the variable ( $\alpha$ ) grows directly proportional to the number of repetitions, the proposed EES is integrated with increasing likelihood. Consequently, the greater the number of repetitions, the further the search is reduced to the region encircling the user's greatest viewpoint. This phase fosters exploitation while simultaneously enabling the discovery of a diverse variety of new viable locations.

According to this method, considerable assistance aims at boosting the search capability of the basic SNS algorithm to surround the best perspective solution, to improve its globally searching possibilities, and to avoid getting locked in a locally optimal solution.

### 3.3. Proposed ASNS with EES for Solving the ORPD Problem

When dealing with the mentioned ORPD problems, the equality and inequality restrictions are considered. The NRA is used to meet the equality criteria that defines power flow balancing equations. It represents the steady-state operation of electricity networks and satisfies the balancing restrictions.

As a result, the NRA, which is employed by MATPOWER, constitutes a critical foundation for showing three-phase power grids [65]. Furthermore, the decision/dependent variable constraints must be preserved. The operational limitations of independent variables in Equations (7)–(9) can be rewritten as follows:

$$VG_i = \begin{cases} VG_i^{\min} & \text{if } VG_i \leq VG_i^{\min} \\ VG_i^{\max} & \text{if } VG_i \geq VG_i^{\max} \end{cases}, \quad i = 1 : NG \tag{27}$$

$$Ta_l = \begin{cases} Ta_l^{\min} & \text{if } Ta_l \leq Ta_l^{\min} \\ Ta_l^{\max} & \text{if } Ta_l \geq Ta_l^{\max} \end{cases}, \quad l = 1 : NT \tag{28}$$

$$Qr_s = \begin{cases} Qr_s^{\min} & \text{if } Qr_s \leq Qr_s^{\min} \\ Qr_s^{\max} & \text{if } Qr_s \geq Qr_s^{\max} \end{cases}, \quad s = 1 : Nr \tag{29}$$

As demonstrated, the variables keep reaching their limits; however, if one of them exceeds the limit, it is reproduced at random within the necessary bounds. Furthermore, the fitness function broadens and penalizes the restrictions of the second classification. As a result, if the user vectors surpass any of the relevant limitations, they will be eliminated in the following round. As stated in Equation (30), those notions can be utilized to create the considered fitness.

$$F = f_j + Pen_1 \sum_{m=1}^{NPQ} \Delta VL_m^2 + Pen_2 \sum_{L=1}^{NPQ} \Delta SF_L^2 + Pen_3 \sum_{k=1}^{NPQ} \Delta QG_k^2 \tag{30}$$

where  $f_j$  indicates each fitness function;  $Pen_1$  is the penalty coefficient for any violation in load voltage;  $Pen_2$  is the penalty coefficient for any violation in reactive power output from generators; and  $Pen_3$  is the penalty coefficient for any violation in line power flow. Where  $\Delta VL_m$ ,  $\Delta SF_L$ , and  $\Delta QG_k$  are presented as:

$$\Delta VL_m = \begin{cases} VL_m^{\min} - VL_m & \text{if } VL_m < VL_m^{\min} \\ VL_m^{\max} - VL_m & \text{if } VL_m > VL_m^{\max} \end{cases} \tag{31}$$

$$\Delta SF_L = SF_L^{\max} - SF_L \text{ if } SF_L > SF_L^{\max} \tag{32}$$

$$\Delta QG_k = \begin{cases} QG_k^{\min} - QG_k & \text{if } QG_k < QG_k^{\min} \\ QG_k^{\max} - QG_k & \text{if } QG_k > QG_k^{\max} \end{cases} \tag{33}$$

Figure 1 displays the stages of the designed ASNS for ORPD.



### 4. Simulation Results

Three distinct standard IEEE grids were utilized as case studies for comparative purposes to investigate the capacity to handle the ORPD challenge as well as the resilience of the suggested ASNS in finding high-quality solutions. The SNS and ASNS algorithms were implemented in the MATLAB software language. The data for three power grids are provided in Table 1, and the entire dataset is derived from [29], while all the limits on control variables used here for all test systems are summarized in Appendix A. The three power grids represent real case studies, where the IEEE 30-bus grid test case represents a simple approximation of the American Electric Power system, while the IEEE 57-bus and IEEE 118-bus grids represent simple approximations of the American Electric Power system in the U.S. Midwest [66].

Table 1. Information from the studied systems.

Case Study	Number of Branches	Number of Loads	Number of Generators	Number of Control Variables	Number of Transformers	Number of Compensators
IEEE 30-bus grid	41	24	6	19	4	9
IEEE 57-bus grid	80	50	7	25	15	3
IEEE 118-bus grid	186	64	54	75	9	12

The SNS and the suggested ASNS algorithms were implemented by adjusting the size of the population and the maximum number of iterations to 50 and 300 for the first grid, 100 and 300 for the second grid, and 100 and 600 for the third grid.

The relation of proposed method parameters to system parameters can be clearly described with Equation (34):

$$Population = \begin{bmatrix} VG_{1,i}(i = 1 : NG) & Ta_{1,l}(l = 1 : NT) & Qr_{1,s}(s = 1 : Nr) \\ VG_{2,i}(i = 1 : NG) & Ta_{2,l}(l = 1 : NT) & Qr_{2,s}(s = 1 : Nr) \\ \vdots & \vdots & \vdots \\ VG_{N,i}(i = 1 : NG) & Ta_{N,l}(l = 1 : NT) & Qr_{N,s}(s = 1 : Nr) \end{bmatrix} \tag{34}$$

The findings of each approach were acquired for each study case by executing 30 tests. The following two cases are being investigated:

- Case 1: Minimization of the TGLs described in Equation (2).
- Case 2: Minimization of the TVD described in Equation (3).
- Case 3: Minimization of the VSI described in Equation (6).

#### 4.1. Results of the First Grid

As illustrated in Figure 2, this grid comprises of 30-bus and 41-branch generators, 4 on-load tap changing transformers, and 9 shunted compensators. The entire dataset for lines, buses, and the limits of reactive power generation is utilized [67,68]. The limits for the generator voltage and tap settings are 1.1000 and 0.9000 p.u., respectively. The limits of voltage for the load buses are considered to be 1.0500 and 0.9500 p.u., respectively. The SNS and proposed ASNS algorithms are implemented in the first case, and the best control settings are presented in Table 2. The basic SNS algorithm reduces TGLs from 5.7960 MW to 4.5208 MW when compared to the initial case; however, the proposed ASNS algorithm achieves the lowest power losses of 4.5206 MW when compared to 5.7960 MW in the initial instance. This is a 22% reduction. The resulting solutions are contrasted with previously reported findings for minimizing the losses and utilizing the same circumstances, as summarized in Table 2, which shows that the proposed ASNS algorithm outperforms numerous strategies in minimizing the TGLs. ILAO [34], SCA [47], WOA [48], HFA [69], QOTLBO [70], CLPSO [22], ABC [28], ALO [28], MPA [50], MFA [71], and AEO [36] achieve

TGLs of 4.5217, 4.7086, 4.5943, 4.529, 4.5594, 4.5615, 4.6110, 4.5900, 4.5335, 4.5340, and 4.5262, respectively.

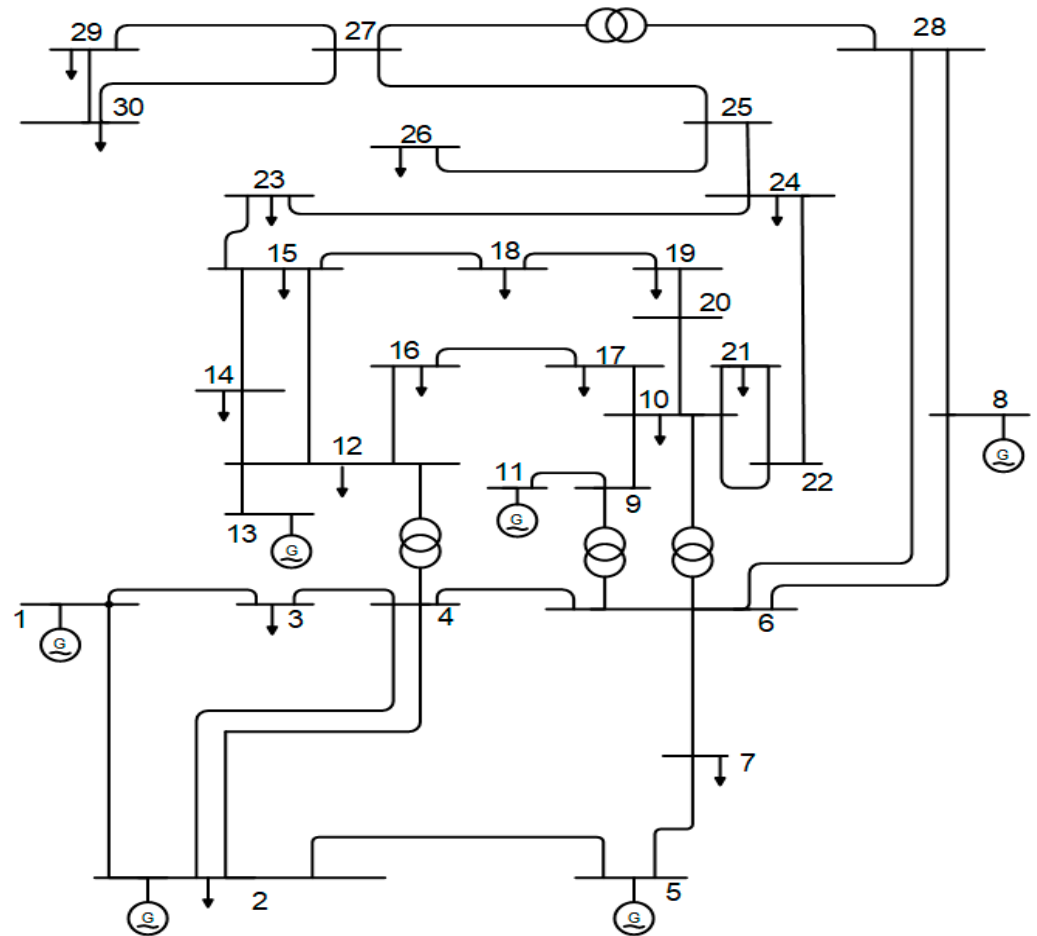


Figure 2. IEEE 30-bus grid [72].

Table 2. Optimal results for Case 1 of the IEEE 30-bus grid.

Variables	Initial Case	SNS	Proposed ASNS	ILAO * [34]	SCA * [47]	WOA * [48]	HFA * [69]
VG <sub>1</sub>	1.0500	1.1000	1.0999	1.1000	1.1000	1.1000	1.1000
VG <sub>2</sub>	1.0400	1.0946	1.0941	1.0944	1.1000	1.0963	1.0543
VG <sub>5</sub>	1.0100	1.0751	1.0741	1.0944	1.0869	1.0789	1.0751
VG <sub>8</sub>	1.0100	1.0768	1.0759	1.0767	1.0870	1.0774	1.0869
VG <sub>11</sub>	1.0500	1.0544	1.0907	1.1000	1.1000	1.0955	1.1000
VG <sub>13</sub>	1.0500	1.0905	1.0824	1.1000	1.0800	1.0929	1.1000
Ta <sub>6-9</sub>	1.0780	1.0746	0.9871	1.0300	1.0500	0.9936	0.9801
Ta <sub>6-10</sub>	1.0690	0.9080	1.0185	0.900	1.0500	0.9867	0.9500
Ta <sub>4-12</sub>	1.0320	1.0000	0.9992	0.9800	1.0500	1.0214	0.9702
Ta <sub>28-27</sub>	1.0680	0.9686	0.9669	0.9600	1.0500	0.9867	0.9700
Qr <sub>10</sub>	0.0000	16.6738	11.8166	4.9900	4.6310	3.1695	4.7003
Qr <sub>12</sub>	0.0000	19.4818	24.57618	5.0000	3.0890	2.0477	4.7061
Qr <sub>15</sub>	0.0000	3.9071	3.7694	5.0000	5.0000	4.2956	4.7007

**Table 2.** *Cont.*

Qr <sub>17</sub>	0.0000	5.5106	5.4730	5.0000	4.6970	2.6782	2.3059
Qr <sub>20</sub>	0.0000	4.0268	3.5115	3.8000	2.1290	4.8116	4.8035
Qr <sub>21</sub>	0.0000	9.7636	10.0785	5.0000	3.1910	4.8163	4.9026
Qr <sub>23</sub>	0.0000	0.9029	1.3975	3.3500	5.0000	3.5739	4.8040
Qr <sub>24</sub>	0.0000	6.8624	6.6386	5.0000	4.3880	4.1953	4.8053
Qr <sub>29</sub>	0.0000	2.2385	2.1505	1.4400	3.5750	2.0009	3.3984
TGLs	5.7960	4.5208	4.5206	4.5217	4.7086	4.5943	4.5290
<b>Variables</b>	<b>QOTLBO * [70]</b>	<b>CLPSO * [22]</b>	<b>ABC * [28]</b>	<b>MFA * [71]</b>	<b>AEO * [36]</b>	<b>ALO * [28]</b>	<b>MPA * [50]</b>
VG <sub>1</sub>	1.1000	1.1000	1.1000	1.1000	1.1000	1.1000	1.1000
VG <sub>2</sub>	1.0942	1.1000	1.0971	1.0943	1.0944	1.0953	1.0949
VG <sub>5</sub>	1.0745	1.0795	1.0866	1.0747	1.0751	1.0767	1.0761
VG <sub>8</sub>	1.0765	1.1000	1.0800	1.0766	1.077	1.0788	1.078
VG <sub>11</sub>	1.1000	1.1000	1.0850	1.1000	1.1000	1.1000	1.0873
VG <sub>13</sub>	1.0999	1.1000	1.1000	1.1000	1.1000	1.1000	1.1000
Ta <sub>6-9</sub>	1.0664	0.9154	1.0700	1.0433	1.0392	1.0100	0.9807
Ta <sub>6-10</sub>	0.9000	0.9000	0.9500	0.9000	0.9000	0.9900	1.0222
Ta <sub>4-12</sub>	0.9949	0.9000	1.0200	0.9791	0.9729	1.0200	0.9765
Ta <sub>28-27</sub>	0.9714	0.9397	1.1000	0.9647	0.9632	1.0000	0.9707
Qr <sub>10</sub>	5.0000	4.9265	5.0000	5.0000	4.9948	4.0000	1.7900
Qr <sub>12</sub>	5.0000	5.0000	0.0000	5.0000	4.9963	2.0000	4.8300
Qr <sub>15</sub>	5.0000	5.0000	2.0000	4.8055	4.8409	4.0000	3.9700
Qr <sub>17</sub>	5.0000	5.0000	5.0000	5.0000	4.9985	3.0000	4.9900
Qr <sub>20</sub>	4.4500	5.0000	4.0000	4.0623	4.2895	2.0000	4.2200
Qr <sub>21</sub>	5.0000	5.0000	5.0000	5.0000	5.0000	4.0000	4.6100
Qr <sub>23</sub>	2.8300	5.0000	4.0000	2.5193	2.6464	3.0000	4.6900
Qr <sub>24</sub>	5.0000	5.0000	5.0000	5.0000	4.9998	5.0000	4.1200
Qr <sub>29</sub>	2.5600	5.0000	4.0000	2.1925	2.2293	5.0000	3.2900
TGLs	4.5594	4.5615	4.611	4.5340	4.5262	4.59	4.5335

\* The techniques in the comparisons are not coded by the authors but are employed by their creators.

Furthermore, the convergent properties of the proposed ASNS and SNS for Case 1 of the IEEE 30-bus grid are depicted in Figure 3. As shown, the curve describes the minimization of the total power losses throughout the iterations, while the small shape provides a zoning on the range [4.5–4.85] MW. The variation of the losses starts at a high value of 6.4500 MW at the fifth iteration and continues decreasing, reaching 4.5892, 4.5313, and 4.5206 MW at iterations 100, 200, and 300, respectively.

Figure 4 depicts the voltage levels acquired employing the SNS and ASNS algorithms. It is confirmed that the voltages on all system buses maintain within the acceptable voltage limitations. In addition, the voltages employed by the suggested SNS and ASNS are significantly higher than in the initial case.

In the second case, the minimization of TVD is considered where the SNS and proposed ASNS algorithms are executed, and the optimal control variables are shown in Table 3. The basic SNS algorithm reduces TVD from 0.8691 p.u. to 0.0846 p.u. when compared to the initial case; however, the proposed ASNS algorithm achieves the lowest TVD value of 0.08435 p.u. when compared to 0.8691 p.u. in the initial instance. This is a 90.3 percent reduction. The resulting solutions are contrasted with previously reported findings for

minimizing the losses and utilizing the same circumstances, as summarized in Table 3, which shows that the proposed ASNS algorithm outperforms numerous strategies in minimizing the TGLs. LAO, ILAO [34], IPG-PSO [73], improved GSA [74], HFA [69], and QOTLBO achieved TVDs of 0.0945, 0.0876, 0.0892, 0.08968, 0.0980, and 0.0856, respectively.

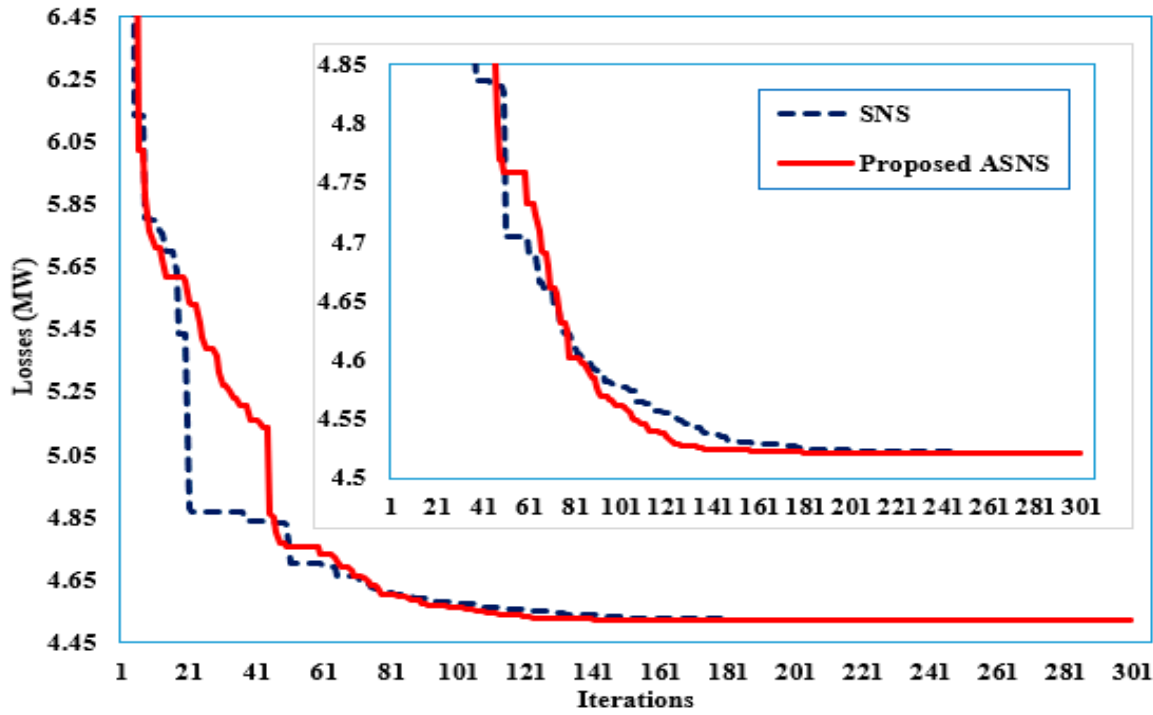


Figure 3. Convergence features of the ASNS and SNS for Case 1 of the IEEE 30-bus grid.

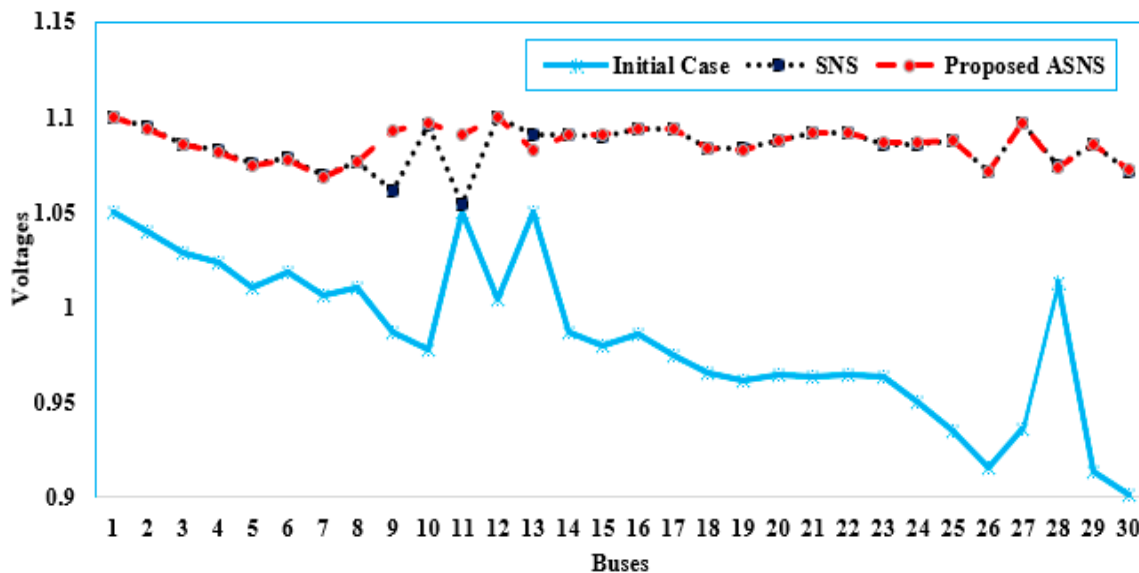


Figure 4. Voltage Profile of the proposed ASNS and SNS for Case 1 of the IEEE 30-bus grid.

Furthermore, the convergent properties of the proposed ASNS and SNS for Case 2 of the IEEE 30-bus grid are depicted in Figure 5. As shown, the curve describes the minimization of the throughput of the iterations, while the small shape provides the range [0.08–0.2] p.u. The TVD starts at a high value of 1.4052 p.u. at the fifth iteration and continues decreasing, reaching 658, 0.1076, 0.09821, and 0.0856 p.u. at iterations 50, 100, 200, and 300, respectively.

**Table 3.** Optimal results for Case 2 of the IEEE 30-bus grid.

	Initial Case	SNS	Proposed ASNS	LAO * [34]	ILAO * [34]	IPG-PSO * [73]	Improved GSA * [74]	HFA * [69]	QOTLBO * [70]
VG <sub>1</sub>	1.0500	1.0040	1.0041	1.0286	0.9942	1.0122	1.0085	1.0035	1.0005
VG <sub>2</sub>	1.0400	1.0000	0.9999	0.9702	0.9563	1.0083	1.0057	1.0164	0.9919
VG <sub>5</sub>	1.0100	1.0000	1.0000	1.0683	1.0689	1.0168	1.0192	1.0195	1.0217
VG <sub>8</sub>	1.0100	1.0023	1.0033	0.9983	0.9919	1.0102	1.0103	1.0182	1.0147
VG <sub>11</sub>	1.0500	1.0001	1.0000	1.0134	1.0650	1.0222	1.0184	0.9823	0.9950
VG <sub>13</sub>	1.0500	1.0000	1.0001	1.0027	1.0436	1.0075	1.0079	1.0155	1.0447
Ta <sub>6-9</sub>	1.0780	1.0074	1.0038	1.0100	1.0900	1.0390	1.0340	0.9900	1.0076
Ta <sub>6-10</sub>	1.0690	1.0992	1.0814	0.9700	0.9400	0.9000	0.9000	0.9000	0.9030
Ta <sub>4-12</sub>	1.0320	1.0196	1.0225	0.9700	1.0400	0.9759	0.9840	0.9800	1.0472
Ta <sub>28-27</sub>	1.0680	0.9946	0.9816	0.9700	0.9800	0.9686	0.9780	0.9600	0.9674
Qr <sub>10</sub>	0.0000	5.9271	12.0240	0.0000	0.0200	5.0000	5.0000	3.2000	4.8700
Qr <sub>12</sub>	0.0000	12.6348	21.6595	2.0400	3.9900	1.8472	5.0000	0.5000	3.0400
Qr <sub>15</sub>	0.0000	9.9277	3.9063	4.9900	4.5000	5.0000	5.0000	4.9000	5.0000
Qr <sub>17</sub>	0.0000	9.3855	5.5190	0.3700	1.0800	0.0026	0.0000	0.1000	0.0000
Qr <sub>20</sub>	0.0000	12.9420	12.6443	4.6400	4.6700	5.0000	5.0000	3.8000	5.0000
Qr <sub>21</sub>	0.0000	16.4084	12.5312	0.0100	0.0200	5.0000	5.0000	5.0000	5.0000
Qr <sub>23</sub>	0.0000	2.3579	3.3287	3.8800	4.9800	4.9915	5.0000	5.0000	5.0000
Qr <sub>24</sub>	0.0000	12.3446	11.7143	4.0100	5.0000	4.9378	5.0000	3.9000	5.0000
Qr <sub>29</sub>	0.0000	6.1102	3.8151	2.5300	4.7900	2.5206	4.9500	1.5000	2.5600
TGLs	5.7960	5.9001	5.7765	5.6154	6.2794	5.7429	5.7500	5.7500	6.4962
TVD	0.8691	0.0846	0.08435	0.0945	0.0876	0.0892	0.08968	0.0980	0.0856

\* The techniques in the comparisons are not coded by the authors but are employed by their creators.

Figure 6 depicts the voltage values acquired employing the proposed SNS and ASNS algorithms. As shown, the voltages employing the suggested SNS and ASNS are significantly better than in the initial case. Based on the suggested SNS and ASNS, the voltages at all buses are very close to the preferred flat voltage of 1 p.u.

In the third case, the minimization of VSI is considered where the SNS and ASNS algorithms are executed, and the optimal control variables are shown in Table 4. The basic SNS algorithm reduces VSI from 0.1720 p.u. to 0.1248 p.u. when compared to the initial case; however, the proposed ASNS algorithm achieves the lowest VSI index of 0.1243 p.u. when compared to 0.1720 p.u. in the initial instance. This is a 27.7 percent reduction.

Table 5 compares the resulting solutions to previously reported findings in order to minimize the VSI objective. Furthermore, the convergent properties of the proposed ASNS and SNS for Case 3 of the IEEE 30-bus grid are depicted in Figure 7. As shown, the curve describes the minimization of the throughput of the iterations, while the small shape is provided on the range [0.1230–0.1480] p.u. The VSI starts at a high value of 0.1511 p.u. at the fifth iteration and continues decreasing, reaching 0.1259, 0.1249, and 0.1243 p.u. at iterations 100, 200, and 300, respectively.

As shown, the proposed ASNS algorithm outperforms numerous strategies in minimizing the VSI. ABC [44], GA [75], SQP, RGA, and CMAES [76] achieve VSIs of 0.1280, 0.1807, 0.1570, 0.1386, and 0.1382, respectively.

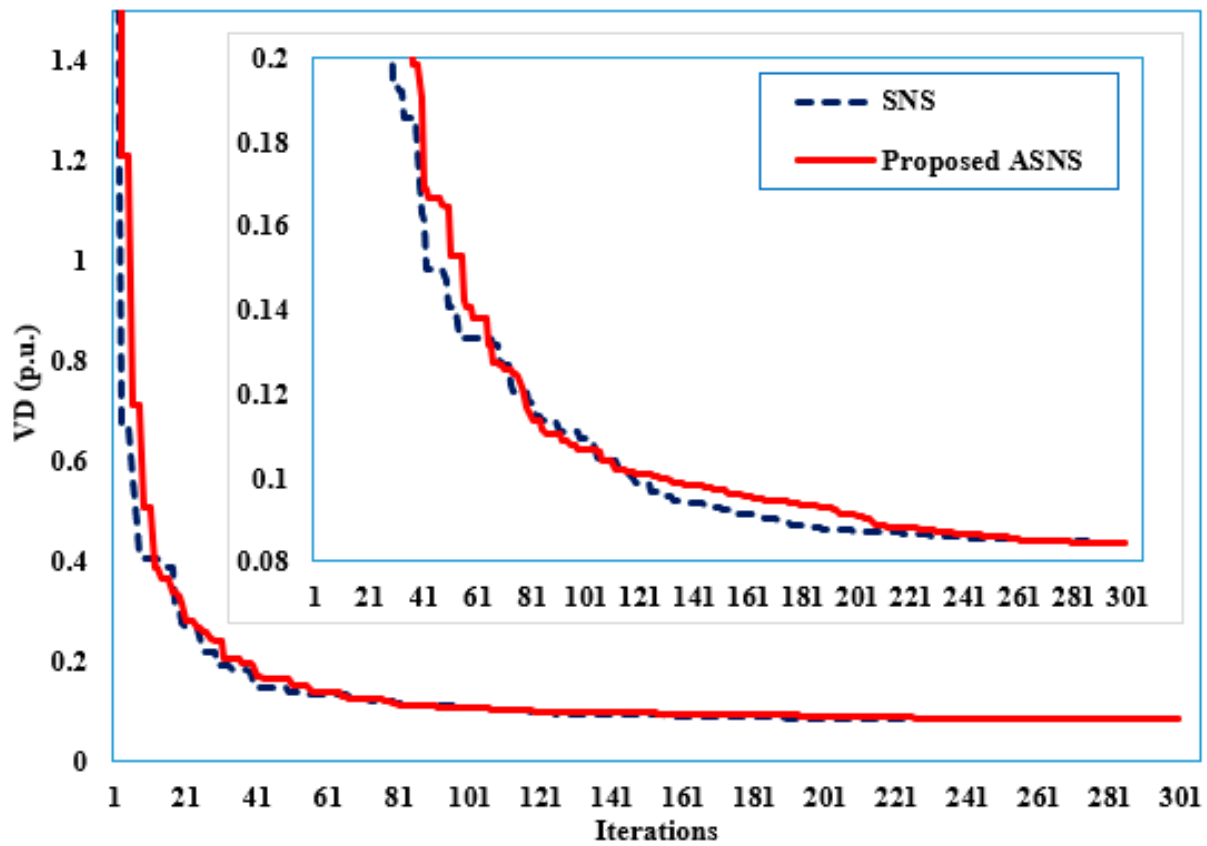


Figure 5. Convergence features of the proposed ASNS and SNS for Case 2 of the IEEE 30-bus grid.

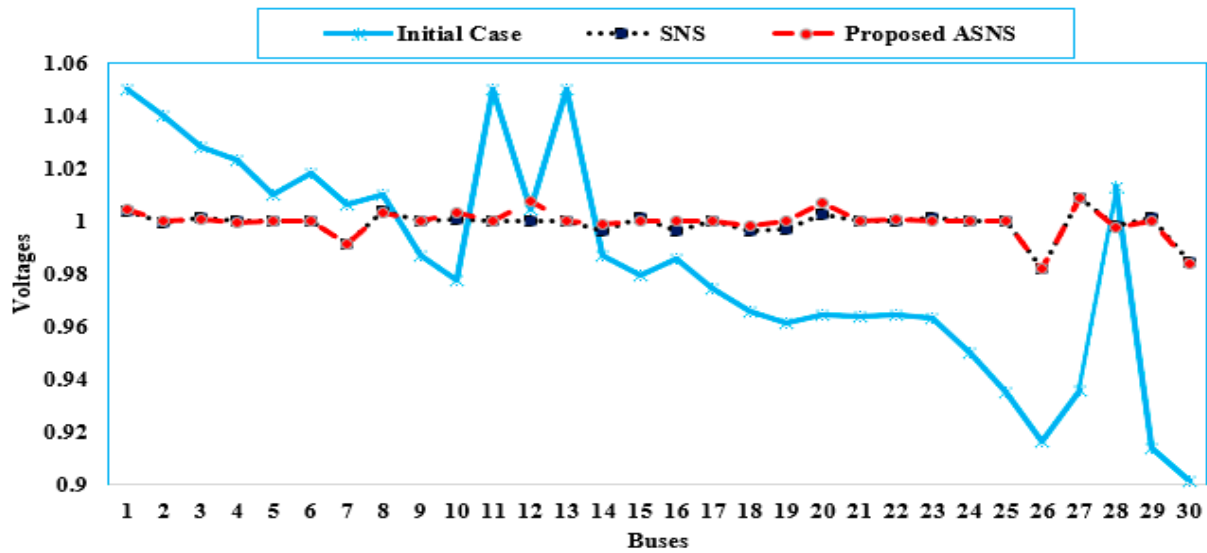


Figure 6. Voltage Profile of the proposed ASNS and SNS for Case 2 of the IEEE 30-bus grid.

On the other side, taking into consideration the tap-changing transformers and shunt capacitors as discrete variables, Table 6 shows the corresponding results of the proposed ASNS algorithm for the three cases studied above. As shown, the outcomes are very similar. For the first case, the TGLs are minimized from 5.7960 to 4.5206 and 4.5222 MW, considering the continuous and discrete nature of tap-changing transformers and shunt capacitors. Furthermore, the TVD is minimized from 0.8691 to 0.08435 and 0.1037 p.u., while the VSI is minimized from 0.1720 to 0.1243 and 0.1241 p.u., respectively, considering the continuous and discrete nature of tap-changing transformers and shunt capacitors.

**Table 4.** Optimal results for Case 3 of the IEEE 30-bus grid.

	Initial Case	SNS	Proposed ASNS
VG <sub>1</sub>	1.0500	1.0990	1.0998
VG <sub>2</sub>	1.0400	1.0933	1.0945
VG <sub>5</sub>	1.0100	1.0671	1.1000
VG <sub>8</sub>	1.0100	1.0869	1.1000
VG <sub>11</sub>	1.0500	1.0998	1.0991
VG <sub>13</sub>	1.0500	1.0997	1.0993
Ta <sub>6-9</sub>	1.0780	0.9896	1.0351
Ta <sub>6-10</sub>	1.0690	0.9355	0.9001
Ta <sub>4-12</sub>	1.0320	1.0076	1.0315
Ta <sub>28-27</sub>	1.0680	0.9545	0.9618
Qr <sub>10</sub>	0.0000	5.5187	0.2385
Qr <sub>12</sub>	0.0000	15.0421	18.0726
Qr <sub>15</sub>	0.0000	0.4000	3.1113
Qr <sub>17</sub>	0.0000	2.2772	8.5207
Qr <sub>20</sub>	0.0000	5.4560	9.9379
Qr <sub>21</sub>	0.0000	4.5358	2.0944
Qr <sub>23</sub>	0.0000	7.4148	0.2498
Qr <sub>24</sub>	0.0000	0.1587	0
Qr <sub>29</sub>	0.0000	0.0183	0.0005
TGLs	5.7960	5.9001	4.9165
TVD	0.8691	2.7656	2.7286
VSI	0.1720	0.1248	0.1243

**Table 5.** Comparative results for Case 3 of the IEEE 30-bus grid.

Method	VSI (p.u.)
Proposed ASNS	0.1243
SNS	0.1248
ABC * [44]	0.1280
GA * [75]	0.1807
SQP * [76]	0.1570
RGA * [76]	0.1386
CMAES * [76]	0.1382

\* The techniques in the comparisons are not coded by the authors but are employed by their creators.

#### 4.2. Results of the Second Grid

The second grid comprises of 57-bus, 80-line, 7-generator and 15 on-load tap changing transformers, and 3 shunted compensators. The limits for the generator voltage and tap settings are 1.1000 and 0.9000 p.u., respectively. The minimum and maximum values for the shunt reactive power injections at buses 18, 25, and 53 are 10.0000, 5.9000, and 6.3000 MVar, respectively.

In the first case, the SNS and proposed ASNS algorithms are implemented, and the best control settings are presented in Table 7. Furthermore, their convergent properties are depicted in Figure 8. The basic SNS algorithm reduces TGLs from 27.8640 MW to 23.9700 MW when compared to the initial case; however, the proposed ASNS algorithm

achieves the lowest power losses of 23.8440 MW when compared to 27.8640 MW in the initial instance. This is a 14.42 % reduction.

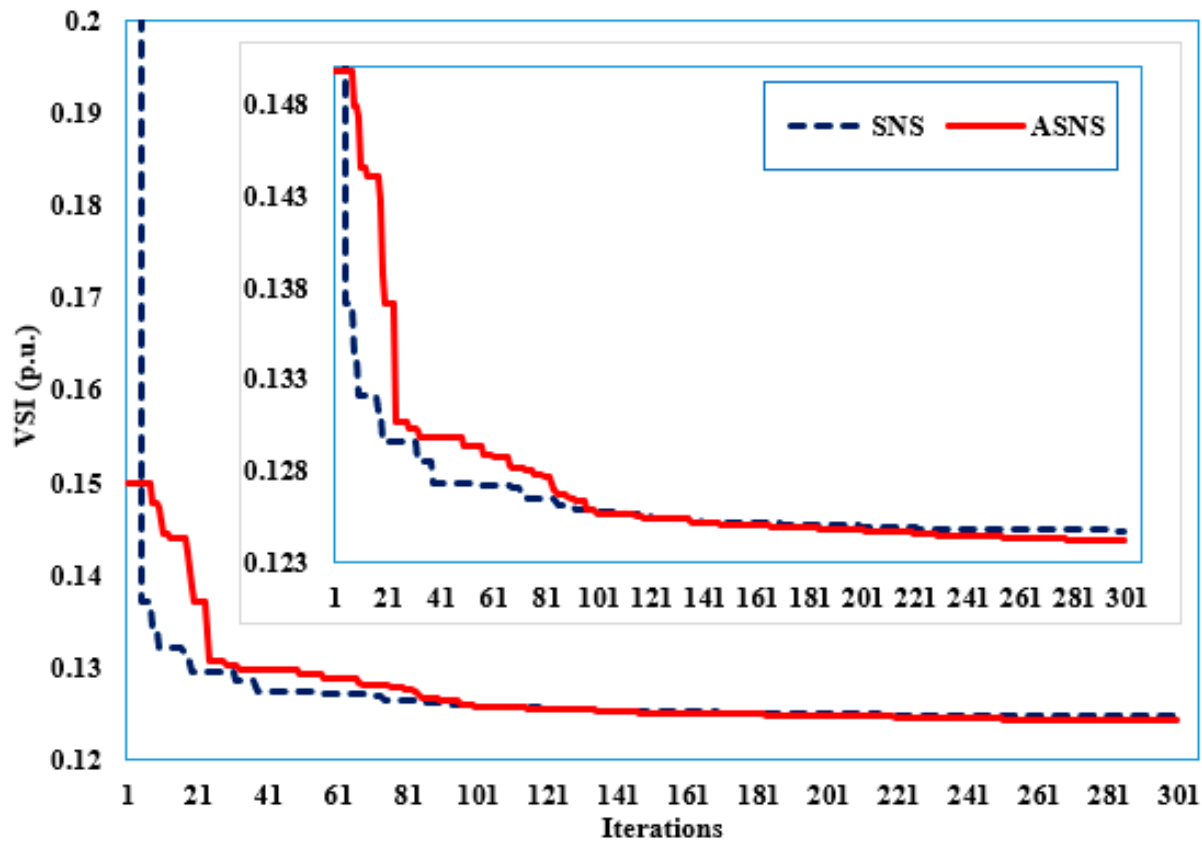


Figure 7. Convergence features of the proposed ASNS and SNS for Case 3 of the IEEE 30-bus grid.

Table 6. Results for Cases 1–3 of the IEEE 30-bus grid considering the continuous and discrete nature of tap-changing transformers and shunt capacitors.

	Initial Case	Case 1 (TGLs Minimization)		Case 2 (TVD Minimization)		Case 3 (VSI Minimization)	
		Continuous	Discrete	Continuous	Discrete	Continuous	Discrete
VG <sub>1</sub>	1.0500	1.0999	1.0999	1.0041	1.0041	1.0998	1.0998
VG <sub>2</sub>	1.0400	1.0941	1.0941	0.9999	0.9999	1.0945	1.0945
VG <sub>5</sub>	1.0100	1.0741	1.0741	1.0000	1.1000	1.1000	1.1000
VG <sub>8</sub>	1.0100	1.0759	1.0759	1.0033	1.0033	1.1000	1.1000
VG <sub>11</sub>	1.0500	1.0907	1.0907	1.0000	1.1000	1.0991	1.0991
VG <sub>13</sub>	1.0500	1.0824	1.0824	1.0001	1.0001	1.0993	1.0993
Ta <sub>6-9</sub>	1.0780	0.9871	0.9800	1.0038	1.1000	1.0351	1.0400
Ta <sub>6-10</sub>	1.0690	1.0185	1.0200	1.0814	1.0800	0.9001	0.9000
Ta <sub>4-12</sub>	1.0320	0.9992	1.0000	1.0225	1.0300	1.0315	1.0300
Ta <sub>28-27</sub>	1.0680	0.9669	0.9700	0.9816	0.9800	0.9618	0.9600
Qr <sub>10</sub>	0.0000	11.8166	12.0000	12.0240	12.0000	0.2385	0.0000
Qr <sub>12</sub>	0.0000	24.5761	25.0000	21.6595	22.0000	18.0726	18.0000
Qr <sub>15</sub>	0.0000	3.7694	4.0000	3.9063	4.0000	3.1113	3.0000
Qr <sub>17</sub>	0.0000	5.4730	5.0000	5.5190	6.0000	8.5207	9.0000

**Table 6.** *Cont.*

	Case 1 (TGLs Minimization)			Case 2 (TVD Minimization)		Case 3 (VSI Minimization)	
	Initial Case	Continuous	Discrete	Continuous	Discrete	Continuous	Discrete
Qr <sub>20</sub>	0.0000	3.5115	4.0000	12.6443	13.0000	9.9379	10.0000
Qr <sub>21</sub>	0.0000	10.0785	10.0000	12.5312	13.0000	2.0944	2.0000
Qr <sub>23</sub>	0.0000	1.3975	1.0000	3.3287	3.0000	0.2498	0.0000
Qr <sub>24</sub>	0.0000	6.6386	7.0000	11.7143	12.0000	0.0000	0.0000
Qr <sub>29</sub>	0.0000	2.1505	2.0000	3.8151	4.0000	0.0005	0.0000
TGLs	5.7960	4.5206	4.5222	5.7765	5.7884	4.9165	4.9185
TVD	0.8691	2.5863	2.5924	0.08435	0.1037	2.7286	2.7249
VSI	0.1720	0.1260	0.1264	0.1511	0.1506	0.1243	0.1241

The minimization of TVD is considered in the second case. Furthermore, the optimal control variables are shown in Table 7, while the convergent properties of the SNS and proposed ASNS algorithms are depicted in Figure 9. The basic SNS algorithm reduces TVD from 1.3586 p.u. to 0.6520 p.u. when compared to the initial case; however, the proposed ASNS algorithm achieves the lowest TVD of 0.6400 p.u. when compared to 1.3586 p.u. in the initial instance. This is a 52.85 percent reduction. For this case, Figure 10 depicts the voltage values acquired employing the proposed SNS and ASNS algorithms. As shown, there have been great improvements in the voltages based on the SNS and ASNS, where the voltages at all buses are very close to the preferred flat voltage of 1.0000 p.u. In addition, the minimum voltage of 0.9359 p.u. at bus 31 is greatly enhanced to be 1.0000 and 0.9800 p.u. based on the SNS and ASNS algorithms, respectively.

**Table 7.** Optimal results for Cases 1–3 of the IEEE 57-bus grid.

	Case 1			Case 2		Case 3	
	Initial Case	SNS	ASNS	SNS	ASNS	SNS	ASNS
VG <sub>1</sub>	1.0400	1.0600	1.0600	1.0096	1.0093	1.0600	1.0398
VG <sub>2</sub>	1.0100	1.0506	1.0508	1.0000	1.0001	1.0359	1.0266
VG <sub>3</sub>	0.9850	1.0448	1.0451	1.0018	1.0021	1.0100	1.0202
VG <sub>6</sub>	0.9800	1.0385	1.0405	1.0003	1.0004	0.9967	1.0234
VG <sub>8</sub>	1.0050	1.0600	1.0600	1.0071	1.0038	1.0196	1.0392
VG <sub>9</sub>	0.9800	1.0282	1.0287	0.9891	0.9876	1.0010	1.0108
VG <sub>12</sub>	1.0150	1.0363	1.0351	1.0206	1.0214	1.0278	1.0406
Ta <sub>4–18</sub>	0.9700	0.9001	1.0015	1.0124	0.9222	0.9042	0.9190
Ta <sub>4–18</sub>	0.9780	1.0994	0.9264	0.9749	1.0603	0.9246	0.9900
Ta <sub>21–20</sub>	1.0430	1.0357	1.0129	0.9808	0.9767	1.1000	1.0978
Ta <sub>24–25</sub>	1.0000	1.0895	1.0221	1.0769	1.0806	0.9129	0.9001
Ta <sub>24–25</sub>	1.0000	0.9340	1.0244	0.9922	1.0543	0.9412	1.0064
Ta <sub>24–26</sub>	1.0430	0.9922	1.0070	0.9984	1.0007	1.0502	1.0629
Ta <sub>7–29</sub>	0.9670	0.9538	0.9476	0.9951	0.9951	0.9134	0.9119
Ta <sub>34–32</sub>	0.9750	0.9598	0.9612	0.9266	0.9165	0.9014	0.9000
Ta <sub>11–41</sub>	0.9550	0.9002	0.9043	0.9016	0.9000	0.9007	0.9003
Ta <sub>15–45</sub>	0.9550	0.9342	0.9335	0.9133	0.9190	0.9124	0.9223

Table 7. Cont.

	Case 1		Case 2		Case 3		
	Initial Case	SNS	ASNS	SNS	ASNS	SNS	ASNS
Ta <sub>14-46</sub>	0.9000	0.9294	0.9206	0.9628	0.9548	0.9003	0.9023
Ta <sub>10-51</sub>	0.9300	0.9318	0.9282	0.9940	0.9974	0.9033	0.9141
Ta <sub>13-49</sub>	0.8950	0.9113	0.9001	0.9000	0.9001	0.9272	0.9060
Ta <sub>11-43</sub>	0.9580	0.9369	0.9175	0.9311	0.9407	0.9156	0.9038
Ta <sub>40-56</sub>	0.9580	1.0019	1.0041	1.0093	0.9895	1.0397	1.0974
Ta <sub>39-57</sub>	0.9800	0.9887	0.9733	0.9099	0.9025	0.9773	1.0901
Ta <sub>9-55</sub>	0.9400	0.9424	0.9400	0.9902	0.9891	0.9580	0.9130
Qr <sub>18</sub>	10.0000	22.4644	12.9690	11.8506	11.4394	10.6182	25.4222
Qr <sub>25</sub>	5.9000	13.2932	14.9441	18.3588	20.0403	0.0006	0.2065
Qr <sub>53</sub>	6.3000	12.5535	12.4807	28.6528	29.1235	22.3590	0.1518
TGLs	27.8640	23.9692	23.8441	28.3819	28.5729	26.1348	26.5536
TVD	1.3586	2.9201	3.4179	0.6520	0.6405	2.4676	2.9997
VSI	0.3000	0.2658	0.2604	0.2990	0.3031	0.2591	0.2542

The minimization of VSI is considered in the third case. Furthermore, the optimal control variables are shown in Table 7, while the convergent properties of the SNS and proposed ASNS algorithms are depicted in Figure 11. The basic SNS algorithm reduces VSI from 0.3000 p.u. to 0.2591 p.u. when compared to the initial case; however, the proposed ASNS algorithm achieves the lowest VSI of 0.2542 p.u. when compared to 0.3000 p.u. in the initial instance, with a reduction of 15.33%.

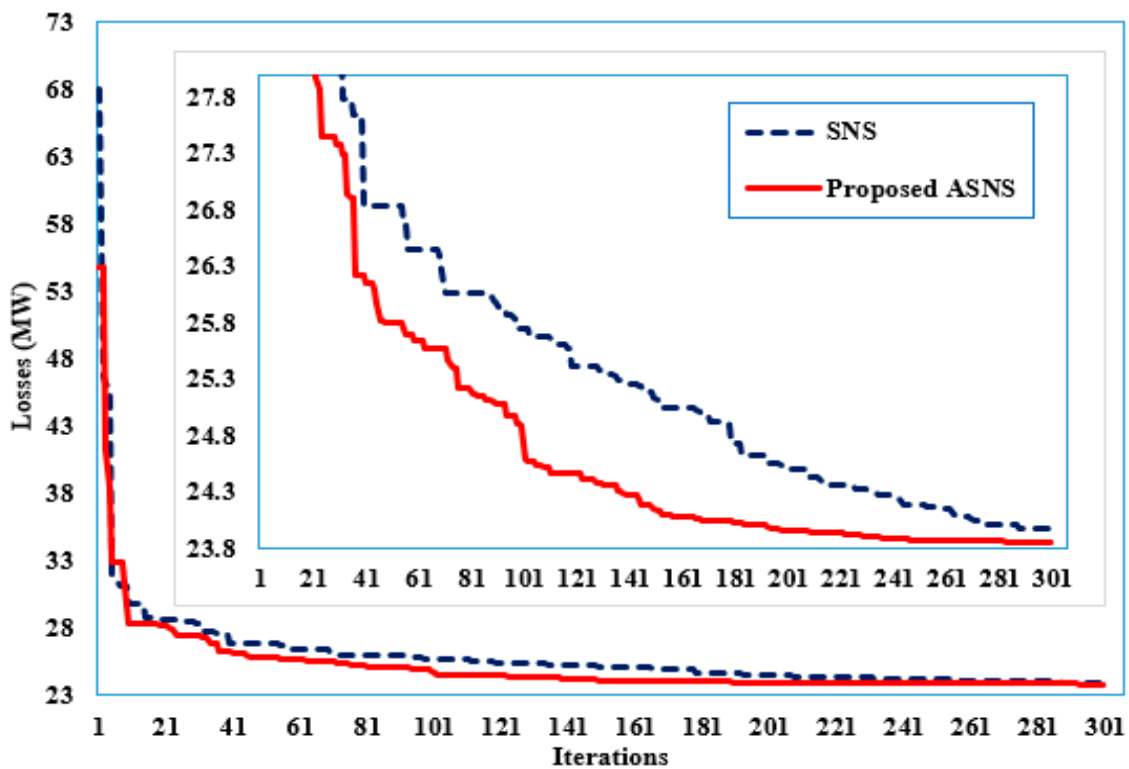


Figure 8. Convergence features of the proposed ASNS and SNS for Case 1 of the IEEE 57-bus grid.

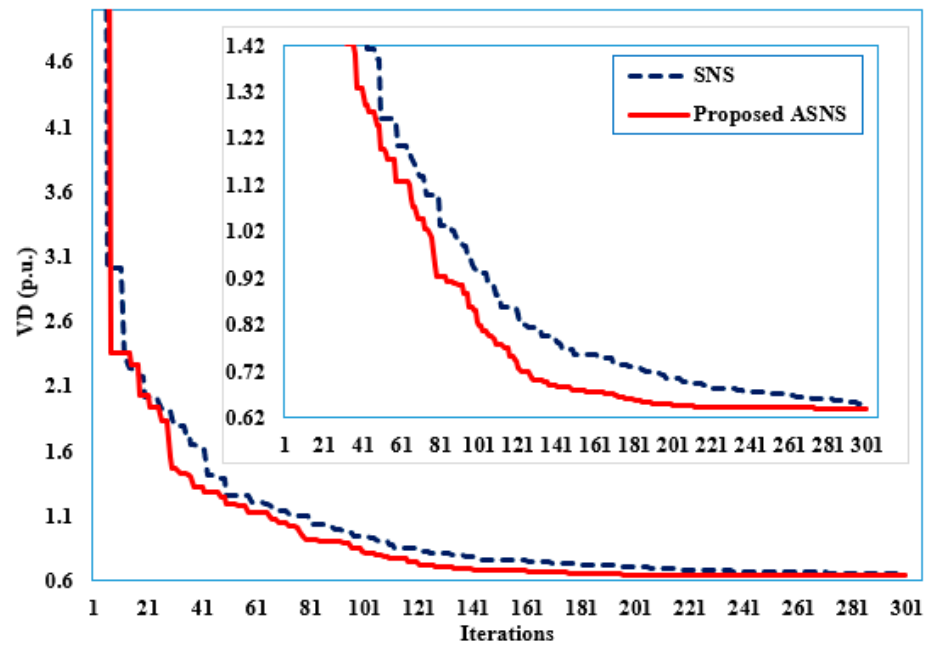


Figure 9. Convergence features of the proposed ASNS and SNS for Case 2 of the IEEE 57-bus grid.

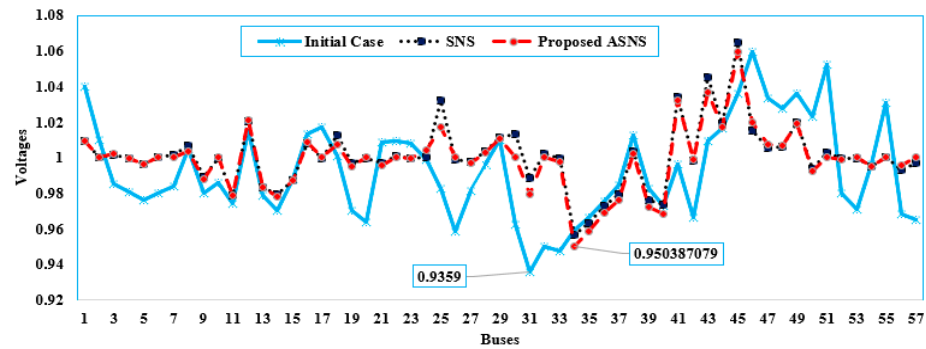


Figure 10. Voltage Profile of the proposed ASNS and SNS for Case 2 of the IEEE 57-bus grid.

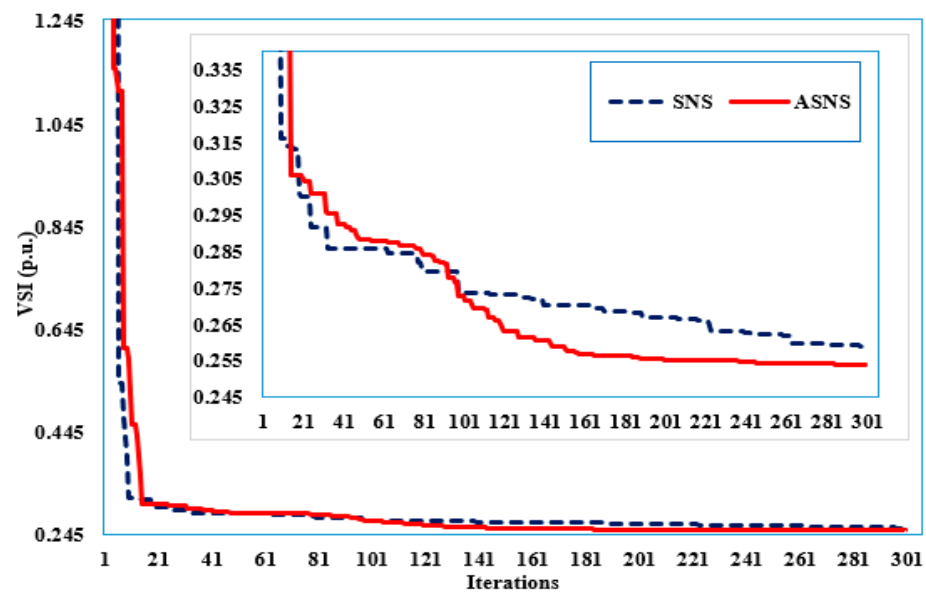


Figure 11. Convergence features of the proposed ASNS and SNS for Case 3 of the IEEE 57-bus grid.

Table 8 illustrates a comparative result of the obtained objectives based on the SNS and ASNS algorithms and other reported findings of several recent algorithms. For the first case, the proposed ASNS obtains the lowest minimum, mean, and maximum TGLs of 23.8441, 23.9695, and 24.4367, respectively. This comparison derives the superior performance of the proposed ASNS against BSA [77], SCA [47], SMA [78], improved SMA [78], SOA [79], ABC [44], and PSO-ICA [26]. Despite the improved SMA [78], which provides the lowest standard deviation of 0.0617, the maximum TGLs recorded by the proposed ASNS of 24.4367 MW are better than the best TGLs obtained by it with 24.5856 MW.

**Table 8.** Comparative results for Cases 1 and 2 of the IEEE 57-bus grid.

<b>Case 1 (TGLs Minimization)</b>				
<b>Method</b>	<b>Min</b>	<b>Mean</b>	<b>Max</b>	<b>Std</b>
Proposed ASNS	23.8441	23.9695	24.4367	0.1119
SNS	23.9692	24.7606	26.1838	0.7348
BSA * [77]	25.3980	24.8382	24.3744	0.2960
SCA * [47]	24.0540	24.6940	25.5270	0.3450
SMA * [78]	24.9009	25.5487	26.0263	0.2346
Improved SMA * [78]	24.5856	24.7079	24.8927	0.0617
SOA * [79]	24.2655	-	-	-
ABC * [44]	24.1025	-	-	-
PSO-ICA * [26]	25.5856	-	-	-
<b>Case 2 (TVD Minimization)</b>				
	<b>Min</b>	<b>Mean</b>	<b>Max</b>	<b>Std</b>
Proposed ASNS	0.6405	0.6653	0.7230	0.0208
SNS	0.6520	0.7018	0.8237	0.0408
OGSA * [80]	0.6982	-	-	-
GB-WCA * [30]	0.6501	-	-	-
WCA * [30]	0.6631	-	-	-
<b>Case 3 (VSI Minimization)</b>				
	<b>Min</b>	<b>Mean</b>	<b>Max</b>	<b>Std</b>
Proposed ASNS	0.2542	0.2586	0.2680	0.0029
SNS	0.2591	0.2650	0.2714	0.0036
HBO * [81]	0.6291	-	-	-
Improved HBO * [81]	0.5085	-	-	-

\* The techniques in the comparisons are not coded by the authors but are employed by their creators.

For the second case, the proposed ASNS obtains the lowest minimum, mean, and maximum TVD of 0.6405, 0.6653, and 0.7230, while the basic SNS achieves counterparts of 0.6520, 0.7018, and 0.8237, respectively. This comparison derives the superior performance of the proposed ASNS against the oppositional GSA (OGSA) [80], GB-WCA [30], and WCA [30], which acquire TVDs of 0.6982, 0.6501, and 0.6631, respectively. For the third case, the proposed ASNS obtains the lowest minimum, mean, and maximum VSIs of 0.2542, 0.2586, 0.2,680, and 0.0029, while the basic SNS achieves counterparts of 0.2591, 0.2650, 0.2714, and 0.0036, respectively. This comparison derives the superior performance of the proposed ASNS against HBO [81], and improved HBO [81] which acquire TVDs of 0.6291 and 0.5085, respectively.

4.3. Results of the Third Grid (Large-Scale Case Study)

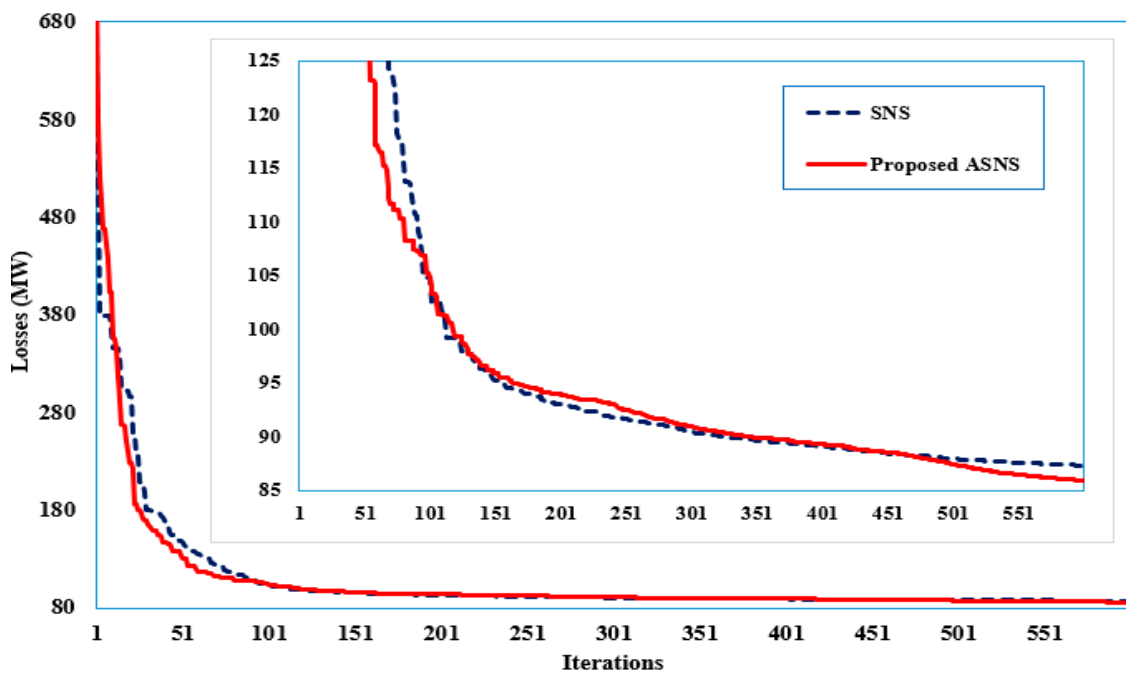
The proposed SNS and ASNS optimizers are implemented to solve the ORPD problem for the large-scale IEEE 118-bus power grid, and to illustrate and appraise their competency in solving larger-scale ORPD challenges. The grid’s complete data can be obtained in [65]. In the first case, the SNS and proposed ASNS algorithms are implemented, and the best control settings are presented in Table 9. Furthermore, their convergent properties are depicted in Figure 12. The proposed ASNS algorithm successfully achieves the minimum TGL of 85.9111 MW, whereas the basic SNS algorithm reduces it to 87.3385 MW.

Table 9. Optimal results for Case 1 of the IEEE 118-bus grid.

Variable	SNS	ASNS	Variable	SNS	ASNS	Variable	SNS	ASNS
VG <sub>1</sub>	0.9506	0.9424	VG <sub>62</sub>	0.9679	0.9720	VG <sub>113</sub>	0.9682	0.9708
VG <sub>4</sub>	0.9809	0.9713	VG <sub>65</sub>	1.0036	1.0597	VG <sub>116</sub>	0.9963	1.0572
VG <sub>6</sub>	0.9715	0.9623	VG <sub>66</sub>	0.9983	0.9985	Ta <sub>8</sub>	1.0466	1.0461
VG <sub>8</sub>	1.0470	1.0478	VG <sub>69</sub>	1.0111	1.0045	Ta <sub>32</sub>	1.0758	1.0498
VG <sub>10</sub>	1.0598	1.0598	VG <sub>70</sub>	0.9683	0.9717	Ta <sub>36</sub>	1.0589	1.0477
VG <sub>12</sub>	0.9673	0.9592	VG <sub>72</sub>	0.9659	0.9679	Ta <sub>51</sub>	1.0330	1.0495
VG <sub>15</sub>	0.9553	0.9562	VG <sub>73</sub>	0.9658	0.9673	Ta <sub>93</sub>	1.0057	1.0796
VG <sub>18</sub>	0.9610	0.9578	VG <sub>74</sub>	0.9562	0.9593	Ta <sub>95</sub>	1.0310	1.0859
VG <sub>19</sub>	0.9543	0.9543	VG <sub>76</sub>	0.9404	0.9400	Ta <sub>102</sub>	0.9728	1.0262
VG <sub>24</sub>	0.9746	0.9899	VG <sub>77</sub>	0.9738	0.9730	Ta <sub>107</sub>	0.9306	1.0104
VG <sub>25</sub>	1.0073	1.0202	VG <sub>80</sub>	0.9860	0.9835	Ta <sub>127</sub>	1.0020	1.0570
VG <sub>26</sub>	1.0591	1.0600	VG <sub>85</sub>	0.9584	0.9726	Qr <sub>34</sub>	4.1112	6.0706
VG <sub>27</sub>	0.9635	0.9713	VG <sub>87</sub>	0.9491	0.9657	Qr <sub>44</sub>	6.7088	1.7000
VG <sub>31</sub>	0.9559	0.9589	VG <sub>89</sub>	0.9730	0.9913	Qr <sub>45</sub>	26.5882	29.9781
VG <sub>32</sub>	0.9589	0.9679	VG <sub>90</sub>	0.9511	0.9627	Qr <sub>46</sub>	1.2823	20.4191
VG <sub>34</sub>	0.9628	0.9547	VG <sub>91</sub>	0.9517	0.9658	Qr <sub>48</sub>	9.3371	14.3187
VG <sub>36</sub>	0.9584	0.9498	VG <sub>92</sub>	0.9583	0.9730	Qr <sub>74</sub>	22.5637	29.9500
VG <sub>40</sub>	0.9554	0.9496	VG <sub>99</sub>	0.9677	0.9691	Qr <sub>79</sub>	29.9349	29.9540
VG <sub>42</sub>	0.9582	0.9545	VG <sub>100</sub>	0.9688	0.9741	Qr <sub>82</sub>	27.7066	28.6906
VG <sub>46</sub>	0.9699	0.9721	VG <sub>103</sub>	0.9631	0.9583	Qr <sub>83</sub>	10.5665	12.9289
VG <sub>49</sub>	0.9847	0.9841	VG <sub>104</sub>	0.9529	0.9445	Qr <sub>105</sub>	18.8040	29.4293
VG <sub>54</sub>	0.9534	0.9491	VG <sub>105</sub>	0.9522	0.9451	Qr <sub>107</sub>	17.9742	27.4281
VG <sub>55</sub>	0.9518	0.9474	VG <sub>107</sub>	0.9497	0.9418	Qr <sub>110</sub>	10.9274	20.1976
VG <sub>56</sub>	0.9518	0.9480	VG <sub>110</sub>	0.9554	0.9468	TGLs	87.3385	85.9111
VG <sub>59</sub>	0.9692	0.9679	VG <sub>111</sub>	0.9629	0.9533	TVD	4.5467	4.8383
VG <sub>61</sub>	0.9710	0.9733	VG <sub>112</sub>	0.9489	0.9400			

For the second case, Table 10 illustrates a comparative result for the obtained objectives based on the SNS and ASNS algorithms and other reported findings of several recent algorithms. As shown, the proposed ASNS obtains the lowest minimum, mean, and maximum TGLs of 85.9111, 87.8445, and 89.7491 MW, respectively. This comparison derives the superior performance of the proposed ASNS against MPA [78], SMA [78], improved SMA [78], OGSA [80], GB-WCA [30], WCA [30], and PSO-ICA [26]. In the second case, the minimization of TVD is considered, and the optimal control variables are shown in Table 11, where the convergent properties of the SNS and proposed ASNS algorithms are

depicted in Figure 13. The proposed ASNS algorithm successfully achieves the minimum TVD of 2.9878 p.u., whereas the basic SNS algorithm reduces it to 3.1799 p.u.



**Figure 12.** Convergence features of the proposed ASNS and SNS for Case 1 of the large-scale IEEE 118-bus grid.

**Table 10.** Comparative results for Case 1 of the IEEE 118-bus grid.

Method	Min	Mean	Max	Std
Proposed ASNS	85.9111	87.8445	89.7491	1.0300
SNS	87.3385	89.0330	90.1690	0.6735
MPA * [78]	115.6104	117.2336	119.3328	1.0301
SMA * [78]	116.6795	118.0399	118.8109	0.5734
Improved SMA * [78]	114.7325	115.2126	115.6699	0.2520
OGSA * [80]	126.9900	-	-	-
GB-WCA * [30]	121.4700	-	-	-
WCA * [30]	131.8300	-	-	-
PSO-ICA * [26]	116.8550	-	-	-

\* The techniques in the comparisons are not coded by the authors but are employed by their creators.

**Table 11.** Optimal results for Case 2 of the IEEE 118-bus grid.

Variable	SNS	ASNS	Variable	SNS	ASNS	Variable	SNS	ASNS
VG <sub>1</sub>	0.9817	0.9813	VG <sub>62</sub>	0.9580	0.9542	VG <sub>113</sub>	0.9970	0.9575
VG <sub>4</sub>	0.9978	1.0008	VG <sub>65</sub>	0.9912	0.9660	VG <sub>116</sub>	0.9558	0.9770
VG <sub>6</sub>	0.9958	0.9998	VG <sub>66</sub>	0.9925	0.9766	Ta <sub>8</sub>	0.9180	0.9664
VG <sub>8</sub>	0.9911	0.9999	VG <sub>69</sub>	0.9995	1.0002	Ta <sub>32</sub>	0.9899	1.0290
VG <sub>10</sub>	0.9984	0.9997	VG <sub>70</sub>	0.9786	0.9878	Ta <sub>36</sub>	1.0241	0.9283
VG <sub>12</sub>	0.9973	1.0000	VG <sub>72</sub>	1.0026	1.0017	Ta <sub>51</sub>	1.0331	1.0032

Table 11. Cont.

Variable	SNS	ASNS	Variable	SNS	ASNS	Variable	SNS	ASNS
VG <sub>15</sub>	0.9541	0.9568	VG <sub>73</sub>	1.0024	1.0001	Ta <sub>93</sub>	1.0512	0.9707
VG <sub>18</sub>	0.9463	0.9508	VG <sub>74</sub>	0.9551	0.9606	Ta <sub>95</sub>	1.0378	0.9477
VG <sub>19</sub>	0.9443	0.9485	VG <sub>76</sub>	0.9405	0.9513	Ta <sub>102</sub>	0.9966	0.9811
VG <sub>24</sub>	1.0074	1.0030	VG <sub>77</sub>	0.9833	0.9938	Ta <sub>107</sub>	0.9489	0.9339
VG <sub>25</sub>	1.0008	1.0048	VG <sub>80</sub>	1.0096	1.0187	Ta <sub>127</sub>	1.0156	1.0137
VG <sub>26</sub>	0.9876	0.9878	VG <sub>85</sub>	0.9644	0.9740	Qr <sub>34</sub>	2.3968	8.3187
VG <sub>27</sub>	0.9833	1.0096	VG <sub>87</sub>	0.9998	1.0012	Qr <sub>44</sub>	27.2772	23.1574
VG <sub>31</sub>	1.0044	1.0019	VG <sub>89</sub>	0.9609	0.9661	Qr <sub>45</sub>	28.9069	29.6803
VG <sub>32</sub>	0.9862	0.9965	VG <sub>90</sub>	1.0034	1.0009	Qr <sub>46</sub>	4.6377	28.9136
VG <sub>34</sub>	0.9545	0.9591	VG <sub>91</sub>	0.9544	0.9503	Qr <sub>48</sub>	5.1663	16.6178
VG <sub>36</sub>	0.9483	0.9522	VG <sub>92</sub>	0.9504	0.9552	Qr <sub>74</sub>	12.7093	9.0686
VG <sub>40</sub>	0.9890	0.9990	VG <sub>99</sub>	0.9905	1.0002	Qr <sub>79</sub>	20.9656	26.9882
VG <sub>42</sub>	1.0040	0.9979	VG <sub>100</sub>	0.9597	0.9668	Qr <sub>82</sub>	24.6778	29.6204
VG <sub>46</sub>	1.0002	1.0131	VG <sub>103</sub>	0.9552	0.9665	Qr <sub>83</sub>	27.8694	29.0008
VG <sub>49</sub>	1.0072	0.9941	VG <sub>104</sub>	0.9483	0.9537	Qr <sub>105</sub>	9.6319	0.1302
VG <sub>54</sub>	0.9524	0.9533	VG <sub>105</sub>	0.9534	0.9548	Qr <sub>107</sub>	7.2698	14.0471
VG <sub>55</sub>	0.9464	0.9506	VG <sub>107</sub>	0.9983	1.0017	Qr <sub>110</sub>	14.8929	26.5572
VG <sub>56</sub>	0.9493	0.9507	VG <sub>110</sub>	0.9483	0.9659	TGLs	100.0307	99.9273
VG <sub>59</sub>	0.9604	0.9552	VG <sub>111</sub>	0.9490	0.9589	TVD	3.1799	2.9878
VG <sub>61</sub>	0.9611	0.9596	VG <sub>112</sub>	0.9560	0.9794			

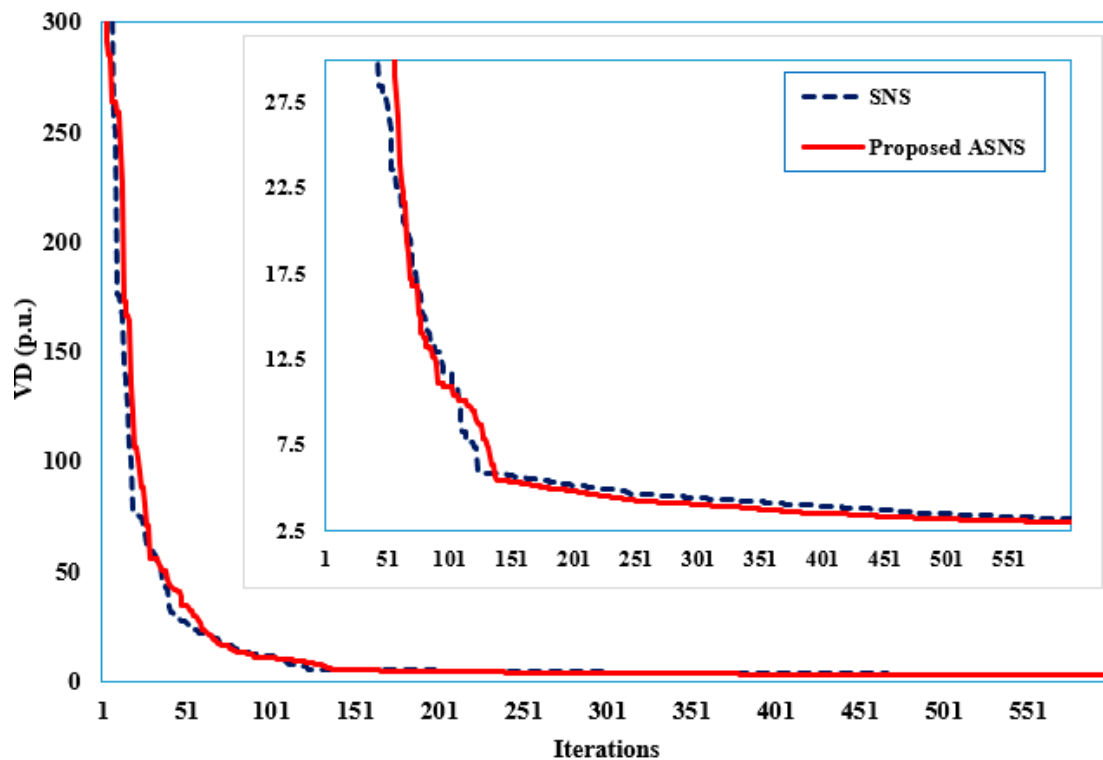


Figure 13. Convergence features of the ASNS and SNS for Case 2 of IEEE 118-bus grid.

The minimization of VSI is considered in the second case. Furthermore, the optimal control variables are shown in Table 12, while the convergent properties of the SNS and proposed ASNS algorithms are depicted in Figure 14. The proposed ASNS algorithm successfully achieves the minimum VSI of 0.0620 p.u., where the basic SNS algorithm reduces it to 0.0645 p.u.

Table 12. Optimal results for Case 3 of the IEEE 118-bus grid.

Variable	SNS	ASNS	Variable	SNS	ASNS	Variable	SNS	ASNS
VG <sub>1</sub>	0.9402	0.9402	VG <sub>62</sub>	0.9506	0.9408	VG <sub>113</sub>	0.9477	0.9658
VG <sub>4</sub>	0.9652	0.9806	VG <sub>65</sub>	0.9521	0.9802	VG <sub>116</sub>	0.9405	0.9453
VG <sub>6</sub>	0.9670	0.9593	VG <sub>66</sub>	0.9920	0.9648	Ta <sub>8</sub>	0.9208	0.9000
VG <sub>8</sub>	0.9572	0.9400	VG <sub>69</sub>	1.0571	1.0544	Ta <sub>32</sub>	0.9891	1.0238
VG <sub>10</sub>	1.0040	0.9866	VG <sub>70</sub>	0.9813	0.9749	Ta <sub>36</sub>	0.9116	0.9758
VG <sub>12</sub>	0.9637	0.9553	VG <sub>72</sub>	0.9408	0.9474	Ta <sub>51</sub>	0.9338	0.9004
VG <sub>15</sub>	0.9446	0.9463	VG <sub>73</sub>	0.9582	0.9427	Ta <sub>93</sub>	0.9425	0.9352
VG <sub>18</sub>	0.9516	0.9429	VG <sub>74</sub>	0.9673	0.9569	Ta <sub>95</sub>	0.9648	0.9470
VG <sub>19</sub>	0.9413	0.9428	VG <sub>76</sub>	0.9408	0.9400	Ta <sub>102</sub>	0.9721	1.1000
VG <sub>24</sub>	0.9461	0.9778	VG <sub>77</sub>	0.9611	0.9628	Ta <sub>107</sub>	0.9031	0.9202
VG <sub>25</sub>	0.9746	0.9471	VG <sub>80</sub>	0.9591	0.9627	Ta <sub>127</sub>	0.9231	0.9042
VG <sub>26</sub>	0.9726	0.9542	VG <sub>85</sub>	0.9403	0.9404	Qr <sub>34</sub>	2.2060	25.8409
VG <sub>27</sub>	0.9576	0.9731	VG <sub>87</sub>	0.9626	0.9533	Qr <sub>44</sub>	29.9001	29.9736
VG <sub>31</sub>	0.9427	0.9457	VG <sub>89</sub>	0.9551	0.9564	Qr <sub>45</sub>	29.6673	29.9865
VG <sub>32</sub>	0.9400	0.9565	VG <sub>90</sub>	0.9468	0.9410	Qr <sub>46</sub>	3.7885	3.6437
VG <sub>34</sub>	0.9516	1.0280	VG <sub>91</sub>	0.9476	0.9561	Qr <sub>48</sub>	3.3209	28.1680
VG <sub>36</sub>	0.9443	1.0238	VG <sub>92</sub>	0.9443	0.9433	Qr <sub>74</sub>	18.1443	14.3624
VG <sub>40</sub>	0.9400	1.0403	VG <sub>99</sub>	0.9679	0.9400	Qr <sub>79</sub>	24.6361	29.8855
VG <sub>42</sub>	1.0600	1.0484	VG <sub>100</sub>	0.9621	0.9513	Qr <sub>82</sub>	23.6569	27.7690
VG <sub>46</sub>	1.0600	1.0591	VG <sub>103</sub>	0.9496	0.9560	Qr <sub>83</sub>	4.1180	0.3922
VG <sub>49</sub>	1.0394	1.0311	VG <sub>104</sub>	0.9407	0.9400	Qr <sub>105</sub>	19.6368	3.2235
VG <sub>54</sub>	0.9482	0.9423	VG <sub>105</sub>	0.9403	0.9451	Qr <sub>107</sub>	16.2616	22.6529
VG <sub>55</sub>	0.9451	0.9400	VG <sub>107</sub>	0.9554	0.9774	Qr <sub>110</sub>	0.2012	5.5425
VG <sub>56</sub>	0.9466	0.9419	VG <sub>110</sub>	0.9430	0.9474	TGLs	107.2403	106.9493
VG <sub>59</sub>	0.9401	0.9414	VG <sub>111</sub>	0.9568	0.9403	TVD	5.8744	5.7535
VG <sub>61</sub>	0.9545	0.9471	VG <sub>112</sub>	0.9401	0.9589	VSI	0.0645	0.0620

#### 4.4. SNS versus Proposed ASNS: Statistical Comparisons

To justify the rate of convergence of the proposed ASNS, the computational times (CPU times) of the SNS and ASNS are tabulated for the IEEE 30-, 57-, and 118-bus systems in Table 13. As shown, there is no significant difference between the SNS and ASNS in the computation time when solving the ORPD problem. In addition, the validation of the generators' reactive power is demonstrated for IEEE 30-, 57-, and 118-bus systems, as stated in Appendix A.

For the sake of assessing the robustness study, the acquired minimum values of the TGLs and TVDs of the 30-runs are analyzed using the SNS and the proposed ASNS algorithms. Their spread and centers for both cases studied of the IEEE 30-, IEEE 57-, and IEEE 118-bus grids are described in Figure 15 via a Box and Whiskers plot. Furthermore, Table 14 displays the detailed robustness indices for Cases 1–3 of the IEEE 30-bus grid, and

the percentage of improvement is evaluated to illustrate the difference between the results achieved by using SNS and ASNS regarding the medium-test system IEEE 30. Additionally, Figure 16 describes the obtained fitness values for both cases for the large-scale IEEE 118-bus grid. To investigate the analysis of the SNS and ASNS in terms of average success rate and convergence characteristics, minimizing the losses (Case 1) for the IEEE 30-bus system is considered. At various percentages of convergence, including 70, 80, 90, and 100%, the absolute difference between the best and worst, its percentage, and the success rate are computed. Table 15 tabulates the related absolute difference between the best and worst and the best percentage, while Figure 17 depicts the regarded success rate. To investigate the robustness of the proposed algorithm parameters on the system behavior, the algorithm parameters are varied in terms of the number of search individuals and the maximum number of iterations, and the success rate is computed for minimizing the losses (Case 1) for the IEEE 30-bus system. The results are tabulated in Table 16.

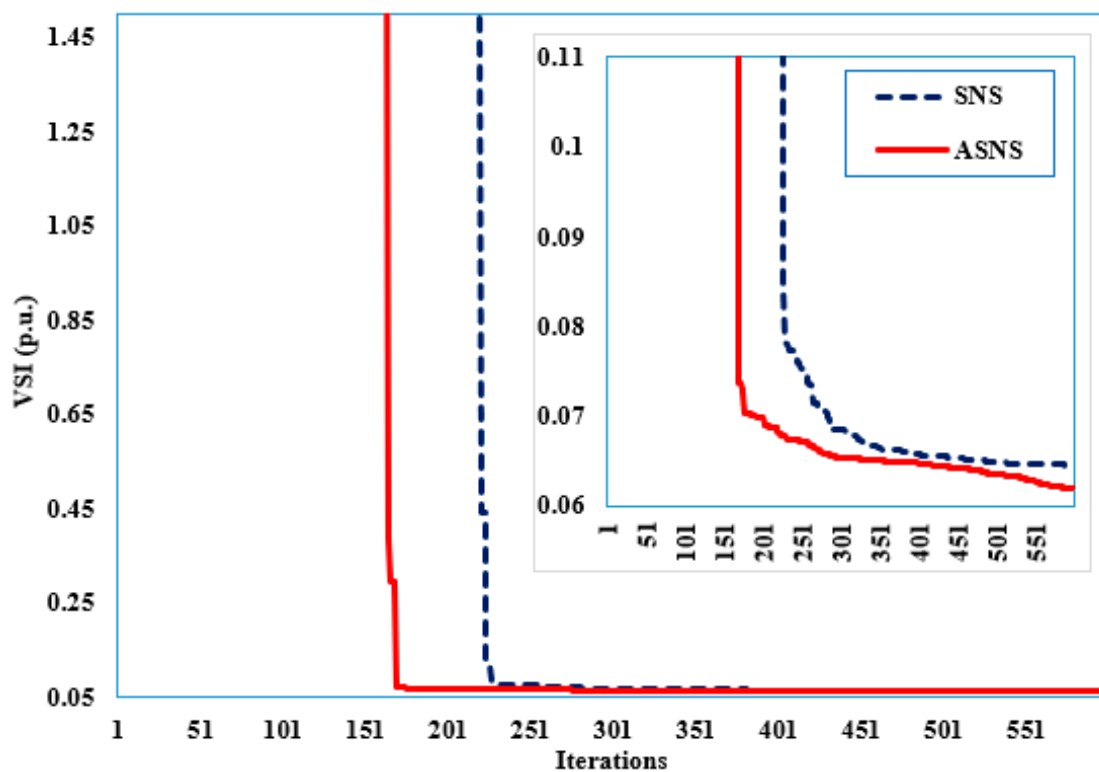


Figure 14. Convergence features of the proposed ASNS and SNS for Case 3 of the IEEE 118-bus grid.

Table 13. Average computational time per iteration using ASNS and SNS.

	SNS	Proposed ASNS
IEEE 30-bus systems	0.7222	0.6690
IEEE 57-bus systems	2.1332	2.1979
IEEE 118-bus systems	4.031	4.1401

Moreover, the effectiveness and performance of the envisaged ASNS and SNS are explored on 25 benchmark functions classified into unimodal, multimodal, fixed, and variable-dimension benchmark functions. Table 17 tabulates their full data in terms of their names, variable lengths, and permissible experiment intervals. The number of search individuals is 30 for the SNS and improved ASNS algorithms, and the maximum number of iterations is 1000. The simulations are performed thirty times. For this purpose, Table 17 provides detailed comparisons in terms of the mean, best, and standard deviation using ASNS and SNS as benchmark functions.

4.5. Discussion Analysis

The proposed ASNS and the original SNS algorithms derive adequate validation of the practical constraints related to the generators’ reactive power, which is demonstrated for IEEE 30-, 57-, and 118-bus systems. Based on the statistical comparisons via Figure 15, the proposed ASNS algorithm shows superior performance compared to the SNS algorithm for all cases studied of the IEEE 30-, IEEE 57-, and IEEE 118-bus grids.

For the IEEE 30-bus grid (Figure 15a), the proposed ASNS algorithm obtains the lowest minimum, mean, and maximum TGLs in the first case of 4.5207, 4.6154, and 4.8987 MW, respectively. Similarly, in the second case, it obtains the lowest minimum, mean, and maximum TVDs of 0.0843, 0.0896, and 0.0983 MW, respectively. Furthermore, the proposed ASNS algorithm provides the smallest standard deviations of TGLs of 0.1254 and TVD of 0.0041, respectively, relative to the SNS algorithm with TGLs of 0.1916 and TVD of 0.005.

As shown in Table 14, great improvement in the standard deviation is obtained with 34.5600, 18.7139, and 17.3804%, respectively, for Cases 1–3. Added to that, a great improvement in the maximum value is obtained with 5.6675, 4.2217, and 1.2360%, respectively, for Cases 1–3. Furthermore, significant improvements in the mean value are obtained with 3.5852, 2.6837, and 1.0783%, respectively, for Cases 1–3. For obtaining the minimum value, the obtained improvement is 0.0036, 0.3085, and 2.1955%, respectively, for Cases 1–3.

Similar findings are attained for the IEEE-57 bus grid (Figure 15b), where the proposed ASNS algorithm provides the smallest standard deviations of TGLs of 0.1119 and TVDs of 0.0207, respectively, relative to the SNS algorithm with TGLs of 0.7348 and TVDs of 0.0407.

For the IEEE 118-bus grid (Figure 15c), the proposed ASNS algorithm provides higher standard deviations of TGLs of 1.0300 and TVDs of 0.3300, respectively, relative to the SNS algorithm with TGLs of 0.6735 and TVDs of 0.3079. Despite that, the majority of the obtained fitness values for both cases are significantly lower than their counterparts using the SNS algorithm, as described in Figure 16.

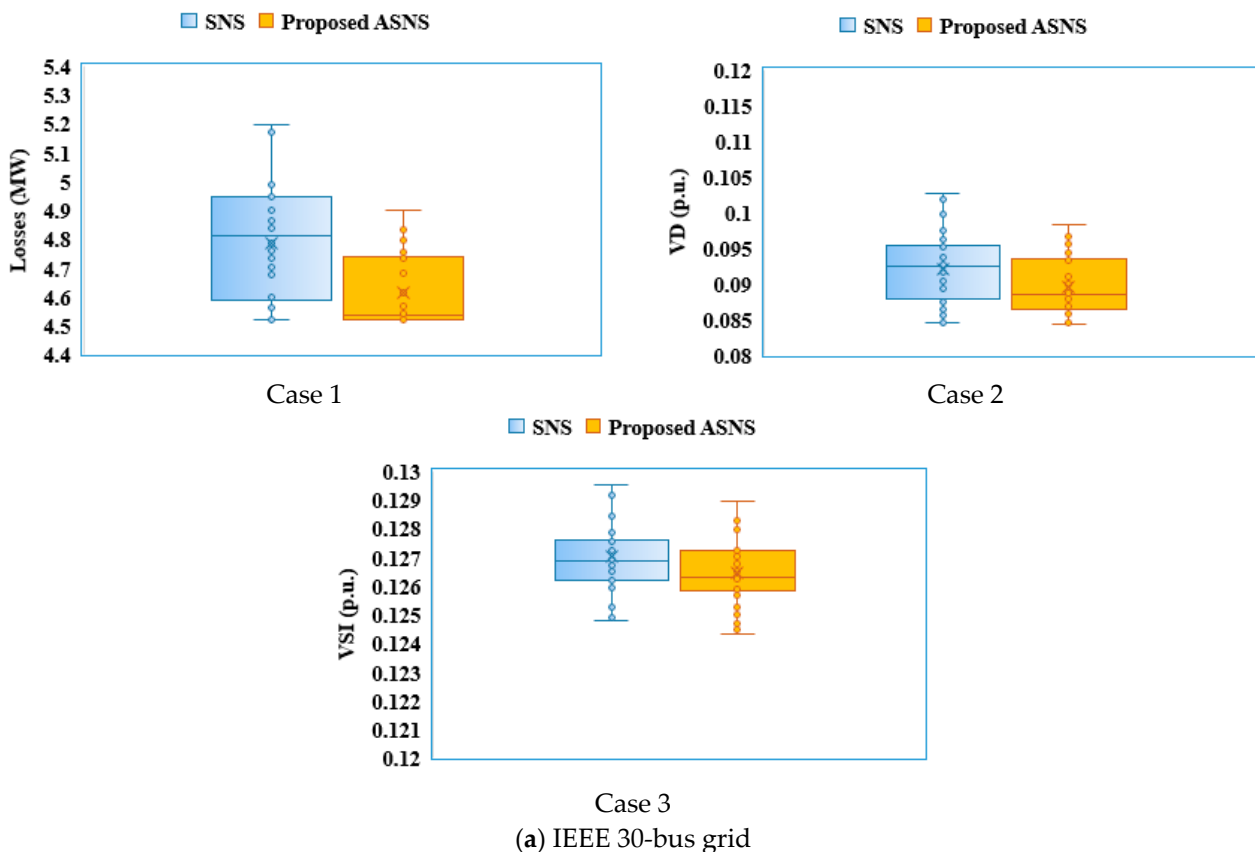


Figure 15. Cont.

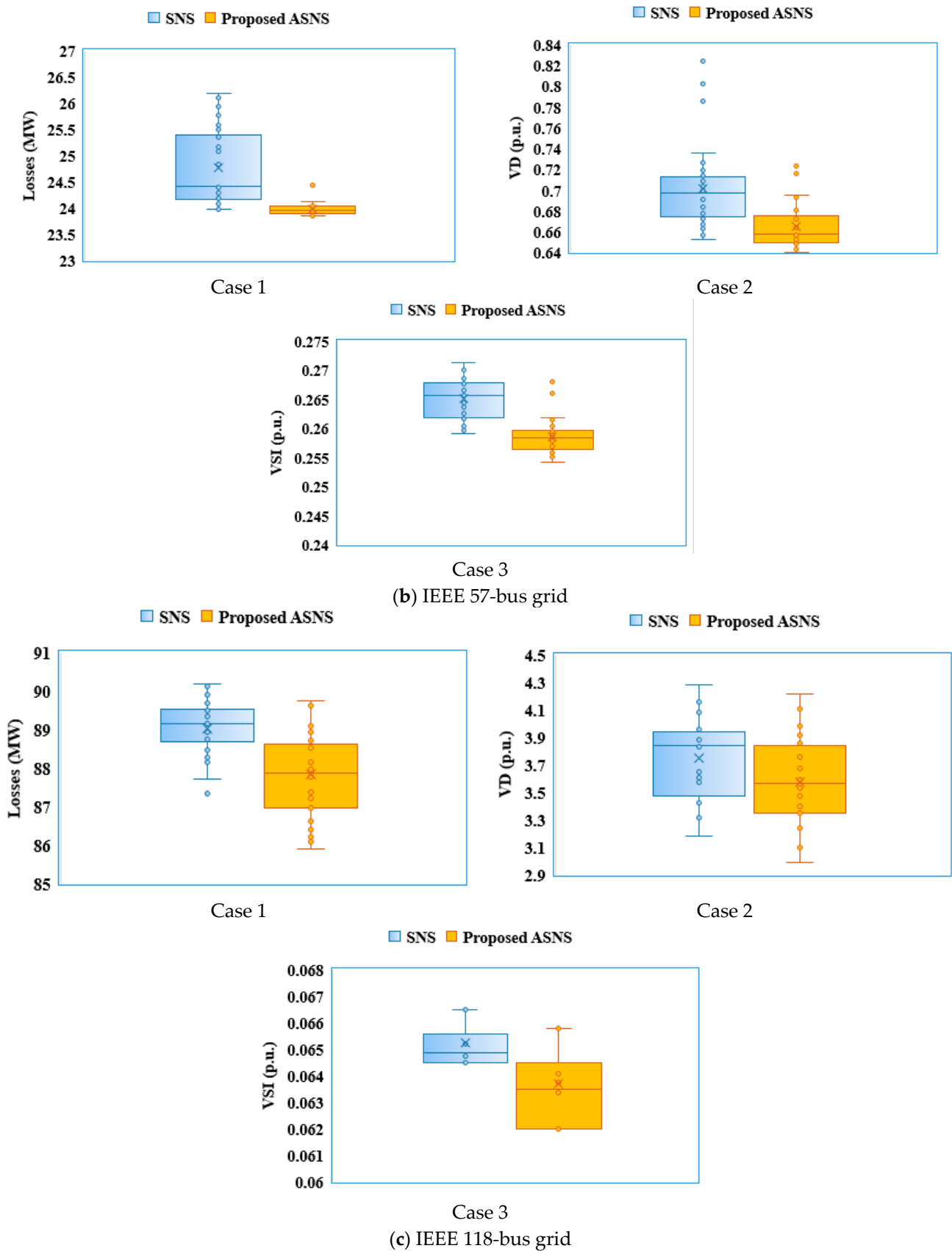
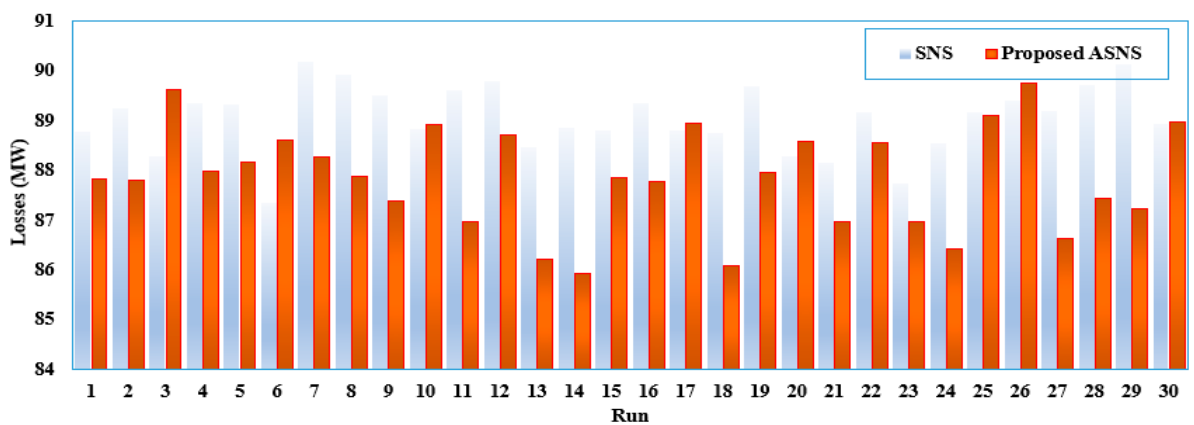


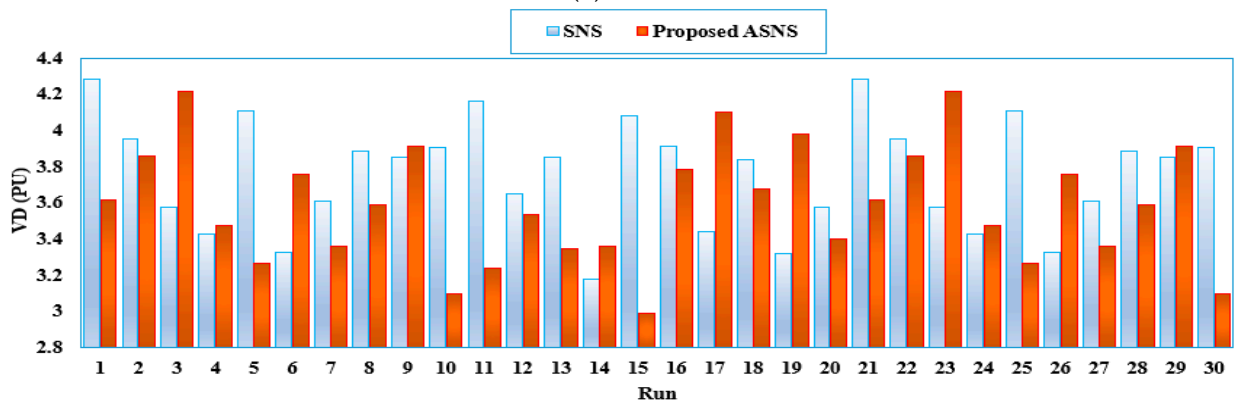
Figure 15. Box and Whiskers plot for the SNS and proposed ASNS of the IEEE 30-, IEEE 57-, and IEEE 118-bus grids.

**Table 14.** Detailed robustness indices for Cases 1-3 of the IEEE 30-bus grid.

	SNS	Proposed ASNS	% Improve	SNS	Proposed ASNS	% Improve	SNS	Proposed ASNS	% Improve
Min.	4.5208	4.5206	0.0036	0.084611	0.08435	0.3085	0.0652	0.0637	2.1955
Mean	4.7870	4.6154	3.5852	0.092111	0.089639	2.6837	0.0665	0.0658	1.0783
Max.	5.1931	4.8988	5.6675	0.102589	0.098258	4.2217	0.2714	0.2679	1.2360
Standard deviation	0.1916	0.1254	34.5600	0.0050	0.0041	18.7139	0.0036	0.0029	17.3804



(a) Case 1



(b) Case 2

**Figure 16.** Obtained fitness values for SNS and proposed ASNS of the IEEE 118-bus grids.

**Table 15.** Absolute difference between the best and worst of SNS and ASNS for minimizing the losses (Case 1) for the IEEE 30-bus system.

	At 100% Convergence		At 90% Convergence		At 80% Convergence		At 70% Convergence	
	SNS	ASNS	SNS	ASNS	SNS	ASNS	SNS	ASNS
Best-worst  (MW)	0.6723	0.3781	0.6991	0.4451	0.7427	0.5441	0.7828	0.6340
Best-worst  (%)	14.8700	8.3600	15.4600	10.0400	16.4300	12.0400	17.3100	14.0800

From both Table 15 and Figure 17, the ASNS provides higher exploitation ability, which is increased with increasing the convergence level. It can be noted that:

- The proposed ASNS always achieves a lower difference percentage compared to the SNS. At 100% convergence, it has 8.36% while the SNS has 14.87%.
- The proposed ASNS always achieves a higher success rate compared to the SNS.

- At 90% and 100% convergence, the proposed ASNS provides approximately 2.5 times the success rate compared to the SNS. At 70% and 80% convergence, the ASNS provides approximately double the success rate of the SNS.

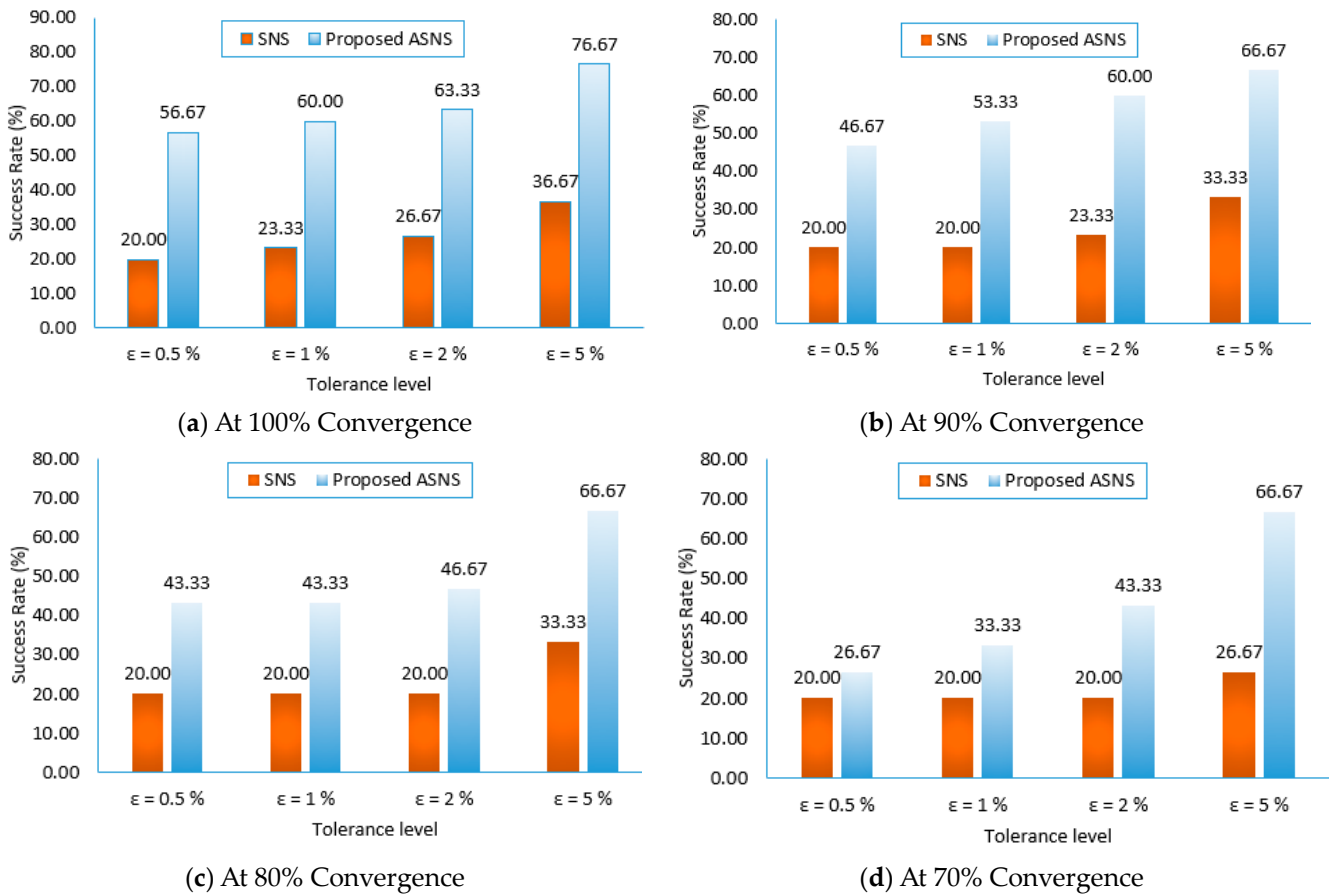


Figure 17. Success rates of SNS and ASNS for Case 1 for the IEEE 30-bus system.

Table 16. Success rates for different values of the ASNS parameters used for minimizing the losses (Case 1) for the IEEE 30-bus system.

Items and Values	Number of Search Individuals				
	15	25	40	50	
Maximum number of iterations	150	0.0000%	10.0000%	16.6667%	20.0000%
	200	3.3334%	16.6667%	16.6667%	33.3334%
	250	3.3334%	16.6667%	20.0000%	56.6667%
	300	6.6667%	16.6667%	26.6667%	76.6667%

Furthermore, as shown in Table 16, increasing the maximum number of iterations increases the success rate. For example, at 50 search individuals, the success rate increases from 20% at 150 iterations to 33.33% at 200 iterations to 56.66% at 250 iterations to 76.66% at 300 iterations. Furthermore, the higher the number of search individuals, the higher the improvement of the success rate. For example, at 300 iterations, the success rate increased from 6.66% at 15 search individuals to 16.66% at 25 search individuals to 26.66% at 40 search individuals to 76.66% at 50 search individuals.

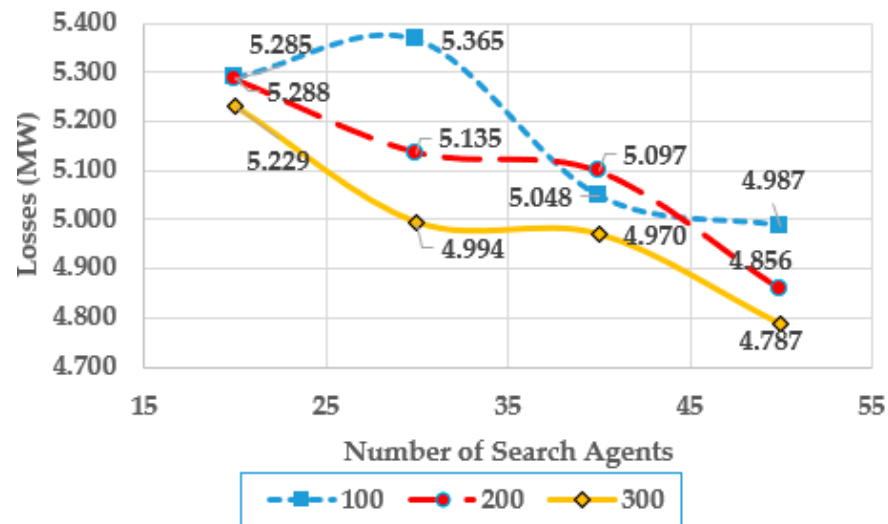
**Table 17.** Comparisons of the mean, best, and standard deviation using ASNS and SNS for benchmark functions.

Fun. No.	Name	Ranges	Dim.	Mean		Standard Deviation		Best	
				ASNS	SNS	ASNS	SNS	ASNS	SNS
F1	Beale	[−4.5, 4.5]	2	0	0	0.0000	0.0000	0	0
F2	Schaffer No. 4	[−100, 100]	2	0.292579	0.292579	$6.9100 \times 10^{-17}$	$6.9100 \times 10^{-17}$	0.292579	0.292579
F3	Salomon	[−100, 100]	30	0.099873	0.099873	$7.7500 \times 10^{-14}$	$1.9300 \times 10^{-9}$	0.099873	0.099873
F4	Leon	[−1.2, 1.2]	2	0	$1.16 \times 10^{-26}$	0.0000	$5.4100 \times 10^{-26}$	0	$1.23 \times 10^{-32}$
F5	Zettl	[−5, 10]	2	−0.00172	−0.00224	$1.0670 \times 10^{-3}$	$1.0970 \times 10^{-3}$	−0.00351	−0.00377
F6	Sphere	[−100, 100]	30	$3.0079 \times 10^{-160}$	$1.1789 \times 10^{-147}$	$9.5051 \times 10^{-160}$	$5.7805 \times 10^{-147}$	$7.1727 \times 10^{-167}$	$2.9501 \times 10^{-152}$
F7	Schwefel’s 2.20	[−100, 100]	30	$1.40367 \times 10^{-81}$	$2.58878 \times 10^{-75}$	$2.3913 \times 10^{-81}$	$6.4732 \times 10^{-75}$	$3.98714 \times 10^{-83}$	$2.44512 \times 10^{-77}$
F8	Brown	[−1, 4]	30	$2.6755 \times 10^{-163}$	$1.4484 \times 10^{-151}$	0.0000	$3.9041 \times 10^{-151}$	$1.3097 \times 10^{-167}$	$4.2958 \times 10^{-156}$
F9	Powell Singular	[−4, 5]	30	$1.69066 \times 10^{-20}$	$3.93264 \times 10^{-10}$	$8.7726 \times 10^{-20}$	$2.1540 \times 10^{-9}$	$4.43765 \times 10^{-30}$	$1.82433 \times 10^{-38}$
F10	Perm 0,D,Beta	[−5, 5]	5	0.062787588	0.111982376	0.086737	0.16016	0.002908003	0.001297683
F11	Sum Squares	[−10, 10]	30	$6.4142 \times 10^{-161}$	$1.1355 \times 10^{-149}$	$2.1289 \times 10^{-160}$	$2.5163 \times 10^{-149}$	$1.4778 \times 10^{-165}$	$2.6613 \times 10^{-152}$
F12	Adjiman	[−1, 2]	2	−1.81123	−1.80019	0.18895	0.20109	−2.02181	−2.0201
F13	Bird	[−2pi, 2pi]	2	−82.1769	−75.2806	20.711	21.134	−106.193	−106.656
F14	Hartman 3	[0, 1]	3	−3.43303	−3.41297	0.27033	0.33938	−3.85014	−3.84113
F15	Cross-in-tray	[−10, 10]	2	−2.01815	−2.01409	0.046780	0.052864	−2.06206	−2.06043
F16	Cross leg table	[−10, 10]	2	−0.00011	−0.00011	$1.4600 \times 10^{-5}$	$1.4900 \times 10^{-5}$	−0.00014	−0.00015
F17	Crowned cross	[−10, 10]	2	0.001192	0.001317	$1.6300 \times 10^{-5}$	$7.0700 \times 10^{-4}$	0.00118	0.001177
F18	Helical Valley	[−10, 10]	3	$6.69 \times 10^{-82}$	$5.79 \times 10^{-46}$	$2.5500 \times 10^{-81}$	$3.1700 \times 10^{-45}$	$6.96 \times 10^{-91}$	$1.61 \times 10^{-64}$
F19	Shubert	[−10, 10]	2	−88.996	−77.3831	41.2951	44.065	−177.796	−179.212
F20	Periodic	[−10, 10]	30	1.044367	1.43648	0.053020	0.081863	1.001063	1.266691
F21	Qing	[−500, 500]	30	1.177906	5.138242	1.4770	13.791	0.103473	0.066978
F22	Alpine N. 1	[−10, 10]	30	$1.83 \times 10^{-83}$	$2.46 \times 10^{-77}$	$2.5400 \times 10^{-83}$	$6.8600 \times 10^{-77}$	$1.26 \times 10^{-85}$	$4.67 \times 10^{-79}$
F23	Xin-She Yang	[−5, 5]	30	$1.79 \times 10^{-75}$	$2.44 \times 10^{-54}$	$9.6700 \times 10^{-75}$	$1.3400 \times 10^{-53}$	$8.23 \times 10^{-94}$	$6.89 \times 10^{-72}$
F24	Wayburn Seader 3	[−500, 500]	2	19.10588	19.10588	$1.4800 \times 10^{-14}$	$1.7800 \times 10^{-14}$	19.10588	19.10588
F25	Dixon and Price	[−10, 10]	30	0.666666677	0.666666692	$2.0899 \times 10^{-8}$	$4.7866 \times 10^{-8}$	0.666666667	0.666666667

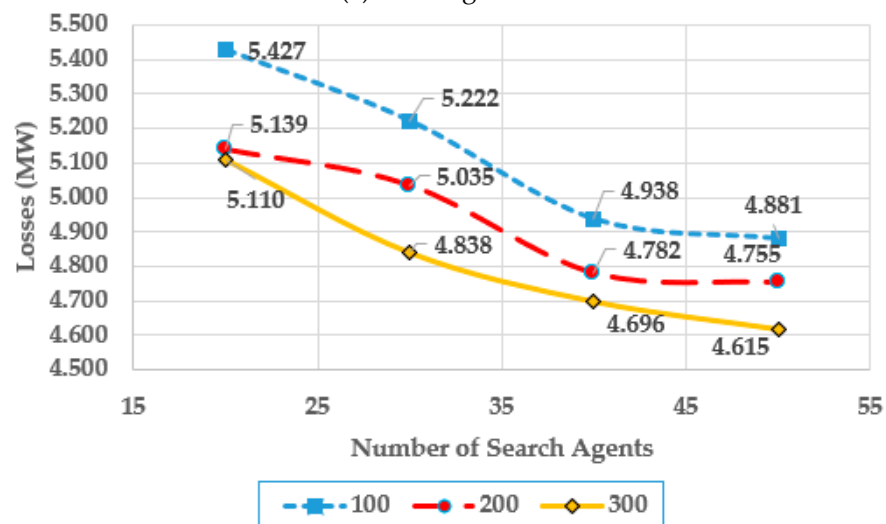
Nevertheless, higher robustness and effectiveness of the proposed improvements to the ASNS algorithm are demonstrated since the proposed ASNS successfully obtains the lowest mean, best, and standard deviation for the majority of the considered benchmark functions, as shown in Table 17.

4.6. Parameter Tuning of SNS and ASNS Algorithms

To demonstrate parameter tuning, the SNS and ASNS algorithms are used with varying numbers of search agents and iterations while power loss minimization is considered. At first, the IEEE 30-bus system is simulated, and Figure 18 describes the corresponding curves for both algorithms.



(a) SNS Algorithm



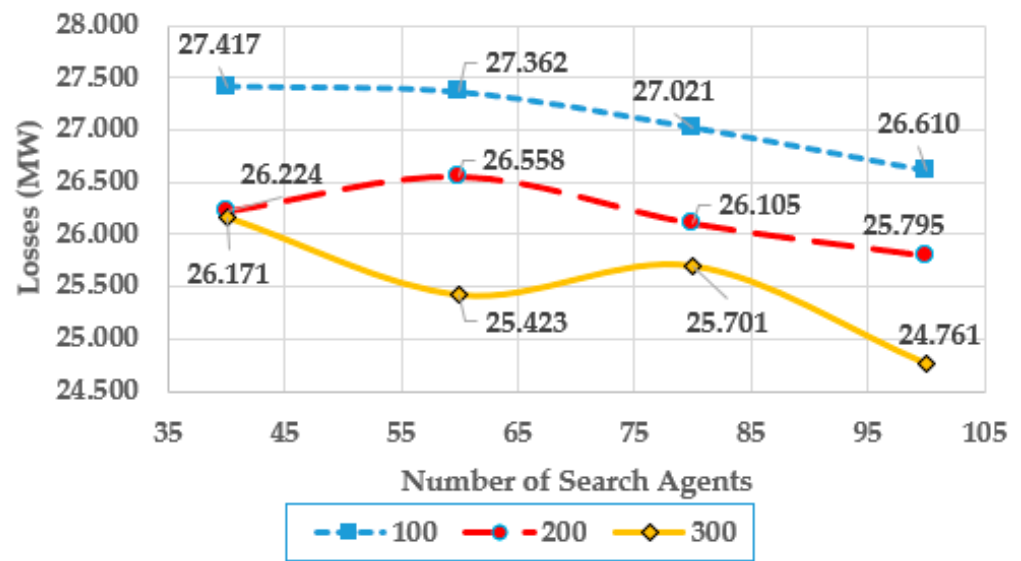
(b) Proposed ASNS Algorithm

Figure 18. Parameter Tuning of SNS and ASNS Algorithms for Case 1 for the IEEE 30-bus system.

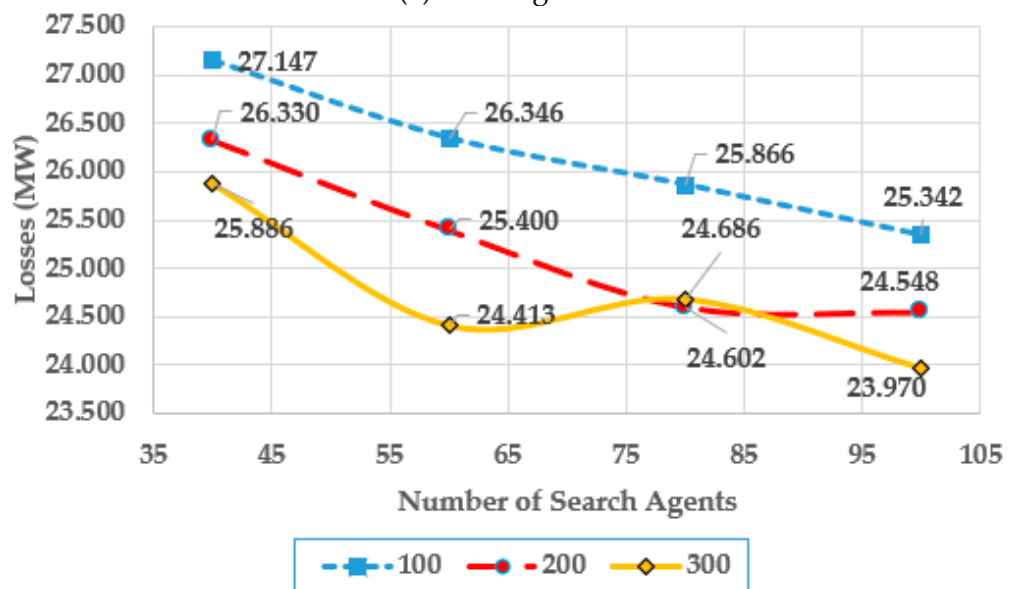
As shown, the lowest power losses are achieved at 50 search agents and 300 iterations for both algorithms. Therefore, the SNS and ASNS algorithms are set to have these characteristics as stated in Table A1 in Appendix A. Furthermore, for both algorithms, increasing the number of iterations and the search agents results in reduced power losses. The proposed ASNS algorithm shows great superiority compared to the original SNS for most of the combinations of the iterations and the search agents. For example, at

300 iterations, the proposed ASNS algorithm provides a reduction in power losses of 2.29, 3.11, 5.51, and 3.59% at a number of search agents of 20, 30, 40, and 50, respectively.

Furthermore, the IEEE 57-bus system is simulated, and Figure 19 depicts the relevant contours for both methods. As demonstrated, the suggested ASNS algorithm outperforms the original SNS for the majority of cycles and search agent combinations. At 100 rounds, the suggested ASNS algorithm reduces power losses by 2.29, 3.71, 4.28, and 4.76% at search agent counts of 30, 40, and 50, respectively. At 200 rounds, the suggested ASNS algorithm reduces power losses by 4.36, 5.76, and 4.83% at search agent counts of 30, 40, and 50, respectively. At 300 rounds, the suggested ASNS algorithm improves power losses by 3.97, 3.95, and 3.19% at search agent counts of 30, 40, and 50, respectively.



(a) SNS Algorithm

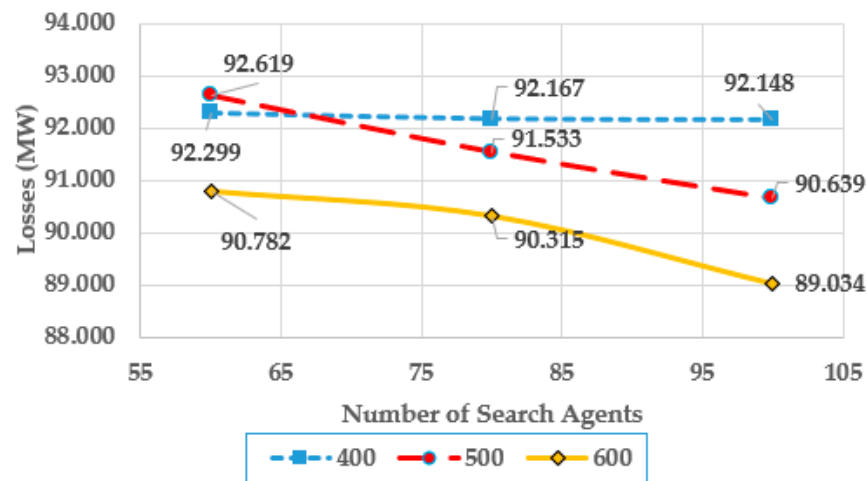


(b) Proposed ASNS Algorithm

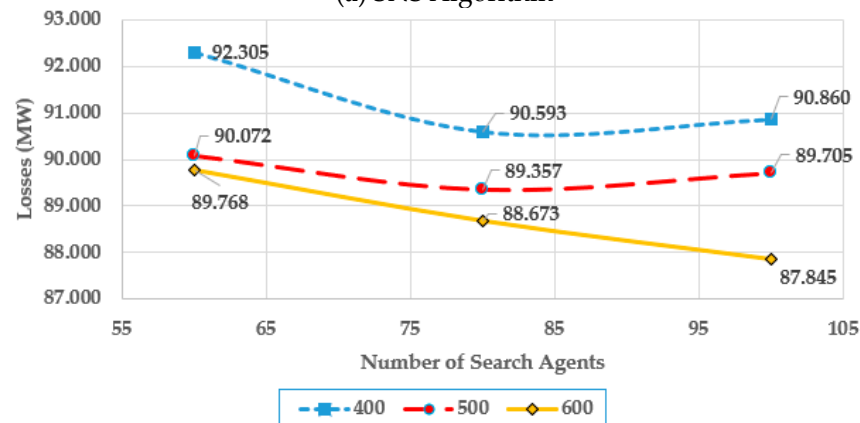
Figure 19. Parameter Tuning of SNS and ASNS Algorithms for Case 1 for IEEE 57-bus system.

Furthermore, for both algorithms, increasing the number of iterations and search agents results in a greater decrease in power losses. Both methods attain the lowest power losses at 100 search agents and 300 iterations. As a result, the SNS and ASNS algorithms are configured to have the traits listed in Table A1 in Appendix A.

Finally, the IEEE 118-bus system is simulated, and Figure 20 describes the corresponding curves for both algorithms.



(a) SNS Algorithm



(b) Proposed ASNS Algorithm

Figure 20. Parameter Tuning of SNS and ASNS Algorithms for Case 1 for the IEEE 118-bus system.

As demonstrated, the suggested ASNS algorithm outperforms the original SNS for most of the repetition and search agent combinations. For example, at 600 iterations, the proposed ASNS algorithm provides a reduction in power losses of 1.12, 1.82, and 1.34% at a number of search agents of 60, 80, and 100, respectively. Furthermore, for both algorithms, increasing the number of iterations and search agents results in a greater decrease in power losses. Both algorithms attain the lowest power losses at 100 search agents and 600 rounds. Therefore, the SNS and ASNS algorithms are set to have these characteristics as stated in Table A1 in Appendix A.

### 5. Conclusions

This study introduces an intelligent optimizer used for finding the optimal scheduling of reactive ORPD power resources (i.e., ASNS). ASNS aims to reduce real power losses and voltage variations while avoiding falling into local optima through two strategies: effective exploitation and adaptable parameter strategies. Simulations were conducted using three standard grids, the IEEE 30-, 57-, and 118-bus. The performance validation across companies' diverse comparisons and statistical analyses is compared with the state of the art. The proposed analysis demonstrates the capability of the ASNS to tackle the ORPD issues with effective and robust performance. The proposed ASNS shows superiority over the state of the art and achieves a great reduction of power losses ( 22%, 14.42%, and 1.62%) and a higher improvement of voltage profiles of 90.3%, 52.85%, and 6.07% for IEEE

30-, IEEE 57-, and IEEE 118-bus grids, respectively. Furthermore, the simulation results show that the ASNS algorithm supports the diversity of populations.

The main objectives that are usually utilized in the ORPD problem are power loss, voltage profile, and voltage stability. Usually, they are very important measures that reflect the technical performance of the steady state operating condition of the system under study. On the other side, some other objectives could be considered for future work, such as reactive power reserve margin maximization and loadability enhancement. Therefore, the future of this study covers two categories. The first aims to solve other complex problems such as OPF for different power system requirements, adding new constraints and limitations for AC/DC grids with the high penetration of renewable energy resources. On the other hand, from the standpoint of solution methodology, developing other optimization algorithms to solve the considered problems.

**Author Contributions:** Conceptualization, A.S.; Methodology, A.S.; Software, S.S. and A.S.; Validation, A.S.; Formal analysis, R.E.-S.; Investigation, S.S. and R.E.-S.; Resources, R.E.-S.; Data curation, A.S. and M.G.; Writing—original draft, A.S.; Writing—review & editing, S.S. and R.E.-S.; Visualization, M.G.; Supervision, S.S. and M.G.; Project administration, M.G.; Funding acquisition, S.S. All authors have read and agreed to the published version of the manuscript.

**Funding:** This research work was funded by Institutional Fund Projects under grant no. (IFPIP: 593-612-1443). The authors gratefully acknowledge technical and financial support from Ministry of Education and King Abdulaziz University, DSR, Jeddah, Saudi Arabia.

**Conflicts of Interest:** The authors declare no conflict of interest.

## Abbreviations

ABC	Artificial bee colony
ABO	Accelerated bio-inspired optimizer
AEO	Artificial ecosystem optimizer
ALO	Ant lion optimizer
APT-FPSO	Adaptive particularly tunable fuzzy particle swarm optimization
ASNS	Augmented social network search
BBO	Biogeography based optimizer
BFA	Bacteria foraging-based algorithm
BSA	Backtracking search algorithm
CAC-DE	Continuous ant colony-based differential evolution
CLPSO	Comprehensive learning particle swarm optimization
CMAES	Covariance matrix adopted evolutionary strategy
CTFWO	Chaotic turbulent flow of water-based optimization
DE	Differential evolution
EES	Effective exploitation strategy
EFA	Enhanced firefly algorithm
ERWCA	Evaporation rate water cycle algorithm
FLP	Fuzzy-based procedure
GA	Genetic algorithm
GB-WCA	Gaussian bare-bones water cycle algorithm
GSA	Gravitational search algorithm
HBO	Heap-based optimizer
HFA	Hybrid firefly algorithm
ICA	Imperialist competitive algorithm
ILAO	improved lightning attachment procedure optimizer
IMPA	Improved version of the marine predator algorithm
IMPA	Improved marine predators' algorithm
IPG-PSO	Improved pseudo-gradient particle swarm optimization
MFA	Moth-flame optimization
MODE	Multi-objective differential evolution
MPA	Marine predators' algorithm

NRA	Newton-Raphson algorithm
OGSA	Oppositional GSA
OPF	Optimal power flow
ORPD	Optimal reactive power dispatch
p.u.	Per unit
PSO	Particle swarm optimization
PSO-TVAC	PSO with time-varying acceleration coefficients
PSO-ICA	Particle swarm optimization-imperialism competitive algorithm
QEA	Quantum-inspired evolutionary algorithm
QODE	Quasi-oppositional differential evolution
QOTLBO	Quasi-oppositional teaching-learning based optimization
RGGA	Real coded genetic algorithm
SBDE	Self-balanced differential evolution
SCA	Sine-cosine Algorithm
SHADE	Successful history-based adaptive Differential Evolution algorithm
SMA	Slime-mould algorithm
SNS	Social network search
SOA	Seeker optimization algorithm
SQP	Sequential quadratic programming
TGLs	Total grid losses
TVD	Total voltage deviation
VSI	Voltage stability index
WCA	Water cycle algorithm
WOA	Whale optimization algorithm
Symbols	
$N$	Number of objectives
$F$	Vector of n objectives
$X_u$ and $X_v$	Dependent and independent variables, respectively
$G_{ij}$	Conductance of every link connecting buses i and j
$\theta, V$ and $N_b$	Phase angle, voltage, and number of buses, respectively
$V_{iew}$	The reference voltage of buses which is taken as 1 p.u.
$L_j$	L-index for each bus j
$\delta_i$ and $\delta_j$	Phase angles of the voltage at buses i and j, respectively
$Y_{LL}$ and $Y_{LG}$	Sub-matrices of Y-Bus matrix
$VG_1, VG_2, \dots, VG_{NG}$	Generator voltages
$Ta_1, Ta_2, \dots, Ta_{NT}$	Transformer tap settings
$Qr_1, Qr_2, \dots, Qr_{Nr}$	Reactive power (VAr) supplied by switched capacitors and reactors
$NG, Nr$ and $NT$	Number of generators, number of the VAr sources, and number of on-load tap transformers, respectively
$VL_1, \dots, VL_{NPQ}$	Load bus voltage magnitudes
$QG_1, QG_2, \dots, QG_{NG}$	VAr outputs of the generators
$SF_1, \dots, SF_{NL}$	Transmission line loadings
$SF_L$ and $NL$	Power flows in line L and the number of transmission lines, respectively
$PL, QL$ and $B_{ij}$	Active and reactive power demand, and mutual susceptance between bus i and j, respectively
$U_i$ and $U_j$	Vectors of the user's view of i and j, respectively
$r_1$ and $r_2$	Random vectors which are, respectively, inside the ranges [0, 1] and [-1, 1].
$U_k$	Randomly selected event vector
$U_{mean}$	Mean vector within a group or commenters of views of friends
$N_{group}$	Number of users in the group
$U_i^d$	The current idea of the user i about each variable d
$U_{best}$	Best viewpoint among the users that get the lowest fitness for every iteration
$LB^d$ and $UB^d$	Lower and upper limits of the variable d, accordingly
$MaxIter$	Maximum number of iterations
$N$	Number of users

### Appendix A

For both SNS and ASNS algorithms, Table A1 describes the number of search individuals and the maximum number of iterations. Furthermore, it contains all the limits on control variables (LB, UB) used herein for all test systems (IEEE 30-, 57-, and 118-bus systems).

**Table A1.** Parameters of the ASNS and SNS for ORPD applications.

Items and Studied Systems		IEEE 30-Bus System	IEEE 57-Bus System	IEEE 118-Bus System
N		50	100	100
MaxIter		300	300	600
Generator voltages (p.u.)	LB	0.9000	0.9000	0.9400
	UB	1.1000	1.1000	1.0600
Tap-changing transformers (p.u.)	LB	0.9000	0.9000	0.9000
	UB	1.1000	1.1000	1.1000
Shunt Capacitors (MVar)	LB	0	0	0
	UB	−30.0000	10.0000, 5.9000, and 6.3000	30.0000

Additionally, Tables A2–A4 provide the generators’ reactive power for IEEE 30-, 57-, and 118-bus systems.

**Table A2.** Generators’ reactive power for the IEEE 30-bus system.

	QMAX	QMIN	Case 1-SNS	Case 1-ASNS	Case 2-SNS	Case 2-ASNS	Case 3-SNS	Case 3-ASNS
QG 1	200	−20	−11.0933	−10.0538	−20	−19.9097	−11.6589	−17.1944
QG 2	100	−20	15.7518	15.5574	−6.8016	−7.4537	15.6506	−13.3928
QG 5	80	−15	24.4079	24.0469	37.5118	37.6167	15.8655	44.3173
QG 8	60	−15	29.0434	28.8129	38.7653	42.4471	56.6655	58.8949
QG 11	50	−10	−2.9666	−0.9345	1.45	0.4212	1.9563	6.465
QG 13	60	−15	−7.156	−13.3821	−2.8688	−4.786	0.4302	1.2194

**Table A3.** Generators’ reactive power for the IEEE 57-bus system.

	QMAX	QMIN	Case 1-SNS	Case 1-ASNS	Case 2-SNS	Case 2-ASNS	Case 3-SNS	Case 3-ASNS
QG 1	200	−140	25.5118	24.9556	−4.5304	−6.9715	110.6362	18.4536
QG 2	50	−17	49.4901	50	43.1114	44.316	19.51	37.5813
QG 3	60	−10	45.8101	47.6413	57.4301	59.8936	9.9011	19.4484
QG 6	25	−8	−5.5959	0.2218	14.8235	18.9114	−2.8447	18.2721
QG 8	200	−140	69.586	66.5433	16.1191	8.1599	48.3652	68.1371
QG 9	9	−3	7.1224	8.8809	9	9	4.8712	1.0238
QG 12	155	−150	75.7926	71.2139	149.7989	154.1204	100.0011	136.6506

Table A4. Generators' reactive power for the IEEE 118-bus system.

	QMAX	QMIN	Case 1-SNS	Case 1-ASNS	Case 2-SNS	Case 2-ASNS	Case 3-SNS	Case 3-ASNS
QG 1	15	−5	14.5662	14.5171	14.6358	14.7846	5.0759	7.8489
QG 4	300	−300	24.0705	−5.7346	−158.184	−42.621	−136.723	−45.0406
QG 6	50	−13	25.8123	20.798	4.1469	24.9696	22.6758	−7.127
QG 8	300	−300	−25.5407	5.4553	179.2201	122.6642	178.53	94.9364
QG 10	200	−147	−100.486	−101.849	−89.6337	−102.598	−26.3501	−21.9034
QG 12	120	−35	53.7451	47.5395	99.0349	108.5367	76.6854	22.4387
QG 15	30	−10	11.6375	17.6951	−4.5287	−9.7037	−0.1446	−4.803
QG 18	50	−16	38.4646	20.1267	−13.2123	−10.1985	35.1172	11.0603
QG 19	24	−8	13.4858	17.414	−5.3478	−1.8856	4.004	−7.1696
QG 24	300	−300	−8.0755	6.6627	24.6526	7.9436	−19.9092	43.1933
QG 25	140	−47	79.5415	50.3089	−19.0465	80.2624	−24.6135	−32.0925
QG 26	1000	−1000	−93.8935	−64.4136	−71.0957	−129.847	33.0448	−69.801
QG 27	300	−300	24.8739	20.9573	12.6348	71.796	70.9331	101.5602
QG 31	300	−300	30.6733	22.3169	91.0509	60.4686	27.5755	14.6481
QG 32	42	−14	9.9814	17.4136	9.809	21.75	−10.8293	7.3427
QG 34	24	−8	13.5709	−6.4994	−1.1196	5.37	4.1177	14.9506
QG 36	24	−8	7.427	2.3472	−3.3417	−5.6468	−6.9791	7.5597
QG 40	300	−300	34.2823	33.0815	68.7116	93.961	−91.0034	50.7242
QG 42	300	−300	19.9429	20.2193	46.3348	33.4737	183.3751	50.9194
QG 46	100	−100	2.58	−11.4573	5.3837	11.5149	41.3022	35.5478
QG 49	210	−85	49.9421	51.7827	139.1609	76.4511	209.4643	207.6757
QG 54	300	−300	42.6336	34.5675	49.4748	53.0367	7.9369	−5.374
QG 55	23	−8	16.2703	11.3564	−6.2283	20.4349	15.1702	10.8474
QG 56	15	−8	1.1199	4.943	−6.5023	−5.3435	−6.4955	5.9728
QG 59	180	−60	91.1813	108.4431	139.8281	96.177	13.9116	28.593
QG 61	300	−100	−2.492	−18.1329	−18.0023	−93.7582	−14.4094	−97.3926
QG 62	20	−20	−3.1049	7.5193	−6.57	−4.0851	−13.9373	−8.5001
QG 65	200	−67	16.9089	3.2103	−8.3426	−66.4617	16.5881	86.23
QG 66	200	−67	−61.7869	−65.5083	−34.4029	−65.5431	−59.0314	49.8348
QG 69	300	−300	−134.618	−110.43	−98.2275	−181.783	161.5133	186.1353
QG 70	32	−10	10.3158	19.4645	1.7462	31.0587	27.373	25.3555
QG 72	100	−100	−6.4364	−13.4015	2.4662	1.6687	−18.189	−22.4441
QG 73	100	−100	−3.1452	−5.3301	26.1035	12.8339	−21.4349	−35.1946
QG 74	9	−6	7.992	6.6092	6.3794	3.7695	6.2625	−3.1613
QG 76	23	−8	22.8668	22.0407	16.8353	20.2507	19.5854	22.912
QG 77	70	−20	56.9625	60.605	36.5389	46.2464	46.2572	46.2732
QG 80	280	−165	39.3082	3.2877	240.1401	230.5782	−123.555	−136.336
QG 85	23	−8	19.3618	18.9086	18.0338	22.8371	14.0021	16.052
QG 87	1000	−100	−0.5023	0.025	12.7369	10.2115	8.7072	5.9641

Table A4. Cont.

	QMAX	QMIN	Case 1-SNS	Case 1-ASNS	Case 2-SNS	Case 2-ASNS	Case 3-SNS	Case 3-ASNS
QG 89	300	−210	0.1398	24.1265	−123.079	−116.085	−28.4652	−11.6247
QG 90	300	−300	51.6318	37.6659	210.6461	199.8874	72.1733	45.8006
QG 91	100	−100	−3.3313	−1.1698	−51.9619	−60.1563	4.301	27.8025
QG 92	9	−3	0.821	5.5476	−2.7115	−2.5073	−0.4118	−2.8518
QG 99	100	−100	−3.6525	−6.4569	34.6788	38.4328	17.4873	−16.9542
QG 100	155	−50	33.2354	59.9011	−40.3621	−49.2498	63.7574	19.4836
QG 103	40	−15	15.7092	2.3865	10.6147	24.2089	1.3529	39.2042
QG 104	23	−8	19.9708	8.3988	9.961	15.3062	17.6745	4.8378
QG 105	23	−8	18.0353	8.845	12.829	−6.6591	3.9311	20.6032
QG 107	200	−200	−1.2282	−10.9052	55.4818	50.2043	16.5422	27.9711
QG 110	23	−8	19.8166	10.8218	0.0812	1.6577	16.7011	16.1153
QG 111	1000	−100	−1.189	−2.5185	−9.6835	−19.4414	6.8634	−19.2893
QG 112	1000	−100	13.0845	12.7739	34.4648	43.5942	18.6459	40.1109
QG 113	200	−100	−7.4075	−12.5293	62.0482	−99.4147	−59.7926	18.0029
QG 116	1000	−1000	27.7889	10.5345	−275.617	4.7293	−66.9456	−155.514

## References

- Chen, X.; Li, K.; Xu, B.; Yang, Z. Biogeography-based learning particle swarm optimization for combined heat and power economic dispatch problem. *Knowl.-Based Syst.* **2020**, *208*, 106463. [\[CrossRef\]](#)
- Acharya, S.; Ganesan, S.; Kumar, D.V.; Subramanian, S. A multi-objective multi-verse optimization algorithm for dynamic load dispatch problems. *Knowl.-Based Syst.* **2021**, *231*, 107411. [\[CrossRef\]](#)
- Naderi, E.; Narimani, H.; Pourakbari-Kasmaei, M.; Cerna, F.V.; Marzband, M.; Lehtonen, M. State-of-the-Art of Optimal Active and Reactive Power Flow: A Comprehensive Review from Various Standpoints. *Processes* **2021**, *9*, 1319. [\[CrossRef\]](#)
- Bentouati, B.; Khelifi, A.; Shaheen, A.M.; El-Sehiemy, R.A. An enhanced moth-swarm algorithm for efficient energy management based multi dimensions OPF problem. *J. Ambient Intell. Humaniz. Comput.* **2020**, *12*, 1–21. [\[CrossRef\]](#)
- Muhammad, Y.; Khan, R.; Raja, M.A.Z.; Ullah, F.; Chaudhary, N.I.; He, Y. Solution of optimal reactive power dispatch with FACTS devices: A survey. *Energy Rep.* **2020**, *6*, 2211–2229. [\[CrossRef\]](#)
- Rezaie, H.; Kazemi-Rahbar, M.H.; Vahidi, B.; Rastegar, H. Solution of combined economic and emission dispatch problem using a novel chaotic improved harmony search algorithm. *J. Comput. Des. Eng.* **2019**, *6*, 447–467. [\[CrossRef\]](#)
- Roy, P.K.; Ghoshal, S.P.; Thakur, S.S. Biogeography based optimization for multi-constraint optimal power flow with emission and non-smooth cost function. *Expert Syst. Appl.* **2010**, *37*, 8221–8228. [\[CrossRef\]](#)
- Hassan, M.H.; Kamel, S.; Abualigah, L.; Eid, A. Development and application of slime mould algorithm for optimal economic emission dispatch. *Expert Syst. Appl.* **2021**, *182*, 115205. [\[CrossRef\]](#)
- Bhadoria, A.; Marwaha, S. Moth flame optimizer-based solution approach for unit commitment and generation scheduling problem of electric power system. *J. Comput. Des. Eng.* **2020**, *7*, 668–683. [\[CrossRef\]](#)
- Shaheen, A.; Ginidi, A.; El-Sehiemy, R.; Elsayed, A.; Elattar, E.; Dorrah, H.T. Developed Gorilla Troops Technique for Optimal Power Flow Problem in Electrical Power Systems. *Mathematics* **2022**, *10*, 1636. [\[CrossRef\]](#)
- Lujano-Rojas, J.M.; Zubi, G.; Dufo-Lopez, R.; Bernal-Agustin, J.L.; Atencio-Guerra, J.L.; Catalao, J.P.S. Embedding quasi-static time series within a genetic algorithm for stochastic optimization: The case of reactive power compensation on distribution systems. *J. Comput. Des. Eng.* **2020**, *7*, 177–194. [\[CrossRef\]](#)
- Deeb, N.I.; Shahidehpour, S.M. An Efficient Technique for Reactive Power Dispatch Using a Revised Linear Programming Approach. *Electr. Power Syst. Res.* **1988**, *15*, 121–134. [\[CrossRef\]](#)
- Venkatesh, S.V.; Liu, W.H.E.; Papalexopoulos, A.D. A Least Squares Solution for Optimal Power Flow Sensitivity Calculation. *IEEE Trans. Power Syst.* **1992**, *7*, 1394–1401. [\[CrossRef\]](#)
- Quintana, V.H.; Santos-Nieto, M. Reactive-power dispatch by successive quadratic programming. *IEEE Trans. Energy Convers.* **1989**, *4*, 425–435. [\[CrossRef\]](#)
- Granville, S. Optimal reactive dispatch through interior point methods. *IEEE Trans. Power Syst.* **1994**, *9*, 136–146. [\[CrossRef\]](#)
- El-Sehiemy, R.A.; El Ela, A.A.A.; Shaheen, A. A multi-objective fuzzy-based procedure for reactive power-based preventive emergency strategy. *Int. J. Eng. Res. Afr.* **2015**, *13*, 91–102. [\[CrossRef\]](#)

17. Vlachogiannis, J.G.; Lee, K.Y. Quantum-inspired evolutionary algorithm for real and reactive power dispatch. *IEEE Trans. Power Syst.* **2008**, *23*, 1627–1636. [[CrossRef](#)]
18. Yoshida, H.; Kawata, K.; Fukuyama, Y.; Takayama, S.; Nakanishi, Y. A Particle swarm optimization for reactive power and voltage control considering voltage security assessment. *IEEE Trans. Power Syst.* **2000**, *15*, 1232–1239. [[CrossRef](#)]
19. Esmin, A.A.A.; Lambert-Torres, G.; Zambroni de Souza, A.C. A hybrid particle swarm optimization applied to loss power minimization. *IEEE Trans. Power Syst.* **2005**, *20*, 859–866. [[CrossRef](#)]
20. Tripathy, M.; Mishra, S. Bacteria foraging-based solution to optimize both real power loss and voltage stability limit. *IEEE Trans. Power Syst.* **2007**, *22*, 240–248. [[CrossRef](#)]
21. Subbaraj, P.; Rajnarayanan, P.N. Optimal reactive power dispatch using self-adaptive real coded genetic algorithm. *Electr. Power Syst. Res.* **2009**, *79*, 374–381. [[CrossRef](#)]
22. Mahadevan, K.; Kannan, P.S. Comprehensive learning particle swarm optimization for reactive power dispatch. *Appl. Soft Comput.* **2010**, *10*, 641–652. [[CrossRef](#)]
23. Sivasubramani, S.; Swarup, K.S. Multi-objective harmony search algorithm for optimal power flow problem. *Int. J. Electr. Power Energy Syst.* **2011**, *33*, 745–752. [[CrossRef](#)]
24. Duman, S.; Sönmez, Y.; Güvenç, U.; Yörükeren, N. Optimal reactive power dispatch using a gravitational search algorithm. *IET Gener. Transm. Distrib.* **2012**, *6*, 563–576. [[CrossRef](#)]
25. Singh, H.; Srivastava, L. Modified Differential Evolution algorithm for multi-objective VAR management. *Int. J. Electr. Power Energy Syst.* **2014**, *55*, 731–740. [[CrossRef](#)]
26. Mehdinejad, M.; Mohammadi-Ivatloo, B.; Dadashzadeh-Bonab, R.; Zare, K. Solution of optimal reactive power dispatch of power systems using hybrid particle swarm optimization and imperialist competitive algorithms. *Int. J. Electr. Power Energy Syst.* **2016**, *83*, 104–116. [[CrossRef](#)]
27. Rajan, A.; Malakar, T. Exchange market algorithm based optimum reactive power dispatch. *Appl. Soft Comput.* **2016**, *43*, 320–336. [[CrossRef](#)]
28. Mouassa, S.; Bouktir, T.; Salhi, A. Ant lion optimizer for solving optimal reactive power dispatch problem in power systems. *Eng. Sci. Technol. an Int. J.* **2017**, *20*, 885–895. [[CrossRef](#)]
29. Li, Z.; Cao, Y.; Van Dai, L.; Yang, X.; Nguyen, T.T. Finding solutions for optimal reactive power dispatch problem by a novel improved antlion optimization algorithm. *Energies* **2019**, *12*, 2968. [[CrossRef](#)]
30. Heidari, A.A.; Ali Abbaspour, R.; Rezaee Jordehi, A. Gaussian bare-bones water cycle algorithm for optimal reactive power dispatch in electrical power systems. *Appl. Soft Comput. J.* **2017**, *57*, 657–671. [[CrossRef](#)]
31. Mouassa, S.; Bouktir, T. Multi-objective ant lion optimization algorithm to solve large-scale multi-objective optimal reactive power dispatch problem. *COMPEL Int. J. Comput. Math. Electr. Electron. Eng.* **2019**, *38*, 304–324. [[CrossRef](#)]
32. Shareef, S.M.; Srinivasa Rao, R. Optimal reactive power dispatch under unbalanced conditions using hybrid swarm intelligence. *Comput. Electr. Eng.* **2018**, *69*, 183–193. [[CrossRef](#)]
33. Lenin, K. Minimization of real power loss by enhanced teaching learning based optimization algorithm Corresponding Author. *Int. J. Robot. Autom.* **2020**, *9*, 1–5. [[CrossRef](#)]
34. Ebeed, M.; Ali, A.; Mosaad, M.I.; Kamel, S. An improved lightning attachment procedure optimizer for optimal reactive power dispatch with uncertainty in renewable energy resources. *IEEE Access* **2020**, *8*, 168721–168731. [[CrossRef](#)]
35. El-Sehiemy, R.A. A novel single/multi-objective frameworks for techno-economic operation in power systems using tunicate swarm optimization technique. *J. Ambient Intell. Humaniz. Comput.* **2022**, *13*, 1073–1091. [[CrossRef](#)]
36. Mouassa, S.; Jurado, F.; Bouktir, T.; Raja, M.A.Z. Novel design of artificial ecosystem optimizer for large-scale optimal reactive power dispatch problem with application to Algerian electricity grid. *Neural Comput. Appl.* **2021**, *33*, 7467–7490. [[CrossRef](#)]
37. Korashy, A.; Kamel, S.; Houssein, E.H.; Jurado, F.; Hashim, F.A. Development and Application of Evaporation Rate Water Cycle Algorithm for Optimal Coordination of Directional Overcurrent Relays. *Expert Syst. Appl.* **2021**, *185*, 115538. [[CrossRef](#)]
38. Qian, J.; Wang, P.; Pu, C.; Chen, G. Joint application of multi-object beetle antennae search algorithm and BAS-BP fuel cost forecast network on optimal active power dispatch problems. *Knowl.-Based Syst.* **2021**, *226*, 107149. [[CrossRef](#)]
39. Liang, R.H.; Wang, J.C.; Chen, Y.T.; Tseng, W.T. An enhanced firefly algorithm to multi-objective optimal active/reactive power dispatch with uncertainties consideration. *Int. J. Electr. Power Energy Syst.* **2015**, *64*, 1088–1097. [[CrossRef](#)]
40. Basu, M. Multi-objective optimal reactive power dispatch using multi-objective differential evolution. *Int. J. Electr. Power Energy Syst.* **2016**, *82*, 213–224. [[CrossRef](#)]
41. Robbins, B.A.; Domínguez-García, A.D. Optimal Reactive Power Dispatch for Voltage Regulation in Unbalanced Distribution Systems. *IEEE Trans. Power Syst.* **2016**, *31*, 2903–2913. [[CrossRef](#)]
42. Basu, M. Quasi-oppositional differential evolution for optimal reactive power dispatch. *Int. J. Electr. Power Energy Syst.* **2016**, *78*, 29–40. [[CrossRef](#)]
43. Nasouri Gilvaei, M.; Jafari, H.; Jabbari Ghadi, M.; Li, L. A novel hybrid optimization approach for reactive power dispatch problem considering voltage stability index. *Eng. Appl. Artif. Intell.* **2020**, *96*, 103963. [[CrossRef](#)]
44. Ettappan, M.; Vimala, V.; Ramesh, S.; Kesavan, V.T. Optimal reactive power dispatch for real power loss minimization and voltage stability enhancement using Artificial Bee Colony Algorithm. *Microprocess. Microsyst.* **2020**, *76*, 103085. [[CrossRef](#)]
45. Biswas, P.P.; Suganthan, P.N.; Mallipeddi, R.; Amaratunga, G.A.J. Optimal reactive power dispatch with uncertainties in load demand and renewable energy sources adopting scenario-based approach. *Appl. Soft Comput.* **2019**, *75*, 616–632. [[CrossRef](#)]

46. Zhang, X.; Yu, T.; Yang, B.; Cheng, L. Accelerating bio-inspired optimizer with transfer reinforcement learning for reactive power optimization. *Knowl.-Based Syst.* **2017**, *116*, 26–38. [CrossRef]
47. Saddique, M.S.; Bhatti, A.R.; Haroon, S.S.; Sattar, M.K.; Amin, S.; Sajjad, I.A.; ul Haq, S.S.; Awan, A.B.; Rasheed, N. Solution to optimal reactive power dispatch in transmission system using meta-heuristic techniques—Status and technological review. *Electr. Power Syst. Res.* **2020**, *178*, 106031. [CrossRef]
48. ben oualid Medani, K.; Sayah, S.; Bekrar, A. Whale optimization algorithm based optimal reactive power dispatch: A case study of the Algerian power system. *Electr. Power Syst. Res.* **2018**, *163*, 696–705. [CrossRef]
49. Suresh, V.; Kumar, S.S. Optimal reactive power dispatch for minimization of real power loss using SBDE and DE-strategy algorithm. *J. Ambient Intell. Humaniz. Comput.* **2020**, 1–15. [CrossRef]
50. Ebeed, M.; Alhejji, A.; Kamel, S.; Jurado, F. Solving the Optimal Reactive Power Dispatch Using Marine Predators Algorithm Considering the Uncertainties in Load and Wind-Solar Generation Systems. *Energies* **2020**, *13*, 4316. [CrossRef]
51. Abd-El Wahab, A.M.; Kamel, S.; Hassan, M.H.; Mosaad, M.I.; AbdulFattah, T.A. Optimal Reactive Power Dispatch Using a Chaotic TurbulentFlow of Water-Based Optimization Algorithm. *Mathematics* **2022**, *10*, 346. [CrossRef]
52. PG, A.K.; Devaraj, D. Hybrid CAC-DE in optimal reactive power dispatch (ORPD) for renewable energy cost reduction. *Sustain. Comput. Inform. Syst.* **2022**, *35*, 100688. [CrossRef]
53. Kien, L.C.; Nguyen, T.T.; Pham, T.D.; Nguyen, T.T. Cost reduction for energy loss and capacitor investment in radial distribution networks applying novel algorithms. *Neural Comput. Appl.* **2021**, *33*, 15495–15522. [CrossRef]
54. Mahfoud, R.J.; Alkayem, N.F.; Sun, Y.; Haes Alhelou, H.; Siano, P.; Parente, M. Improved hybridization of evolutionary algorithms with a sensitivity-based decision-making technique for the optimal planning of shunt capacitors in radial distribution systems. *Appl. Sci.* **2020**, *10*, 1384. [CrossRef]
55. Jamil Mahfoud, R.; Sun, Y.; Faisal Alkayem, N.; Haes Alhelou, H.; Siano, P.; Shafie-khah, M. A novel combined evolutionary algorithm for optimal planning of distributed generators in radial distribution systems. *Appl. Sci.* **2019**, *9*, 3394. [CrossRef]
56. Le Kien, C.; Tuyet, Y.; Thi, N.; Phan, T.M.; Nguyen, T.T. Finding Optimal Solutions for the Placement of Reactive and Active Power Generation Components in Distribution Networks Using a High-Performance Metaheuristic Algorithm. *Int. Trans. Electr. Energy Syst.* **2022**, *2022*, 3761983.
57. Talatahari, S.; Bayzidi, H.; Saraee, M. Social Network Search for Global Optimization. *IEEE Access* **2021**, *9*, 92815–92863. [CrossRef]
58. El-Sehiemy, R.; Elsayed, A.; Shaheen, A.; Elattar, E.; Ginidi, A. Scheduling of Generation Stations, OLTC Substation Transformers and VAR Sources for Sustainable Power System Operation Using SNS Optimizer. *Sustainability* **2021**, *13*, 11947. [CrossRef]
59. Shaheen, A.M.; Elsayed, A.M.; Ginidi, A.R.; El-Sehiemy, R.A.; Elattar, E. Enhanced social network search algorithm with powerful exploitation strategy for PV parameters estimation. *Energy Sci. Eng.* **2022**, *10*, 1398–1417. [CrossRef]
60. Shaheen, A.M.; El-Sehiemy, R.A.; Farrag, S.M. A novel framework for power loss minimization by modified wind driven optimization algorithm. In Proceedings of the 2018 International Conference on Innovative Trends in Computer Engineering, ITCE, Aswan, Egypt, 19–21 February 2018; IEEE: Piscataway, NJ, USA, 2018; Volume 2018.
61. Shaheen, A.M.; Spea, S.R.; Farrag, S.M.; Abido, M.A. A review of meta-heuristic algorithms for reactive power planning problem. *Ain Shams Eng. J.* **2018**, *9*, 215–231. [CrossRef]
62. Shaheen, A.M.; El-Sehiemy, R.A.; Farrag, S.M. Optimal reactive power dispatch using backtracking search algorithm. *Aust. J. Electr. Electron. Eng.* **2016**, *13*, 200–210. [CrossRef]
63. Ginidi, A.R.; Elsayed, A.M.; Shaheen, A.M.; Elattar, E.E.; El-Sehiemy, R.A. A Novel Heap based Optimizer for Scheduling of Large-scale Combined Heat and Power Economic Dispatch. *IEEE Access* **2021**, *9*, 83695–83708. [CrossRef]
64. Shaheen, A.M.; Elsayed, A.M.; Ginidi, A.R.; El-Sehiemy, R.A.; Elattar, E. A heap-based algorithm with deeper exploitative feature for optimal allocations of distributed generations with feeder reconfiguration in power distribution networks. *Knowl.-Based Syst.* **2022**, *241*, 108269. [CrossRef]
65. Zimmerman, R.D.; Murillo-Sánchez, C.E.; Thomas, R.J. Matpower [Software]. Available online: <https://matpower.org> (accessed on 2 January 2023).
66. Electric Grid Test Cases. Available online: <https://electricgrids.engr.tamu.edu/electric-grid-test-cases/> (accessed on 2 January 2023).
67. Elattar, E.E.; Shaheen, A.M.; Elsayed, A.M.; El-Sehiemy, R.A. Optimal power flow with emerged technologies of voltage source converter stations in meshed power systems. *IEEE Access* **2020**, *8*, 166963–166979. [CrossRef]
68. Ghasemi, M.; Taghizadeh, M.; Ghavidel, S.; Aghaei, J.; Abbasian, A. Solving optimal reactive power dispatch problem using a novel teaching-learning-based optimization algorithm. *Eng. Appl. Artif. Intell.* **2015**, *39*, 100–108. [CrossRef]
69. Rajan, A.; Malakar, T. Optimal reactive power dispatch using hybrid Nelder-Mead simplex based firefly algorithm. *Int. J. Electr. Power Energy Syst.* **2015**, *66*, 9–24. [CrossRef]
70. Mandal, B.; Roy, P.K. Optimal reactive power dispatch using quasi-oppositional teaching learning based optimization. *Int. J. Electr. Power Energy Syst.* **2013**, *53*, 123–134. [CrossRef]
71. Mei, R.N.S.; Sulaiman, M.H.; Mustafa, Z.; Daniyal, H. Optimal reactive power dispatch solution by loss minimization using moth-flame optimization technique. *Appl. Soft Comput.* **2017**, *59*, 210–222.
72. Shaheen, A.M.; El-Sehiemy, R.A.; Ginidi, A.R.; Ghoneim, S.S.M.; Alharthi, M.M. Multi-objective jellyfish search optimizer for efficient power system operation based on multi-dimensional OPF framework. *Energy* **2021**, *237*, 121478. [CrossRef]

73. Polprasert, J.; Ongsakul, W.; Dieu, V.N. Optimal reactive power dispatch using improved pseudo-gradient search particle swarm optimization. *Electr. Power Compon. Syst.* **2016**, *44*, 518–532. [[CrossRef](#)]
74. Chen, G.; Liu, L.; Zhang, Z.; Huang, S. Optimal reactive power dispatch by improved GSA-based algorithm with the novel strategies to handle constraints. *Appl. Soft Comput.* **2017**, *50*, 58–70. [[CrossRef](#)]
75. Devaraj, D.; Roselyn, J.P. Genetic algorithm based reactive power dispatch for voltage stability improvement. *Int. J. Electr. Power Energy Syst.* **2010**, *32*, 1151–1156. [[CrossRef](#)]
76. Jeyadevi, S.; Baskar, S.; Babulal, C.K.; Willjuice Iruthayarajan, M. Solving multiobjective optimal reactive power dispatch using modified NSGA-II. *Int. J. Electr. Power Energy Syst.* **2011**, *33*, 219–228. [[CrossRef](#)]
77. Shaheen, A.M.; El-Sehiemy, R.A.; Farrag, S.M. Integrated Strategies of Backtracking Search Optimizer for Solving Reactive Power Dispatch Problem. *IEEE Syst. J.* **2018**, *12*, 424–433. [[CrossRef](#)]
78. Wei, Y.; Zhou, Y.; Luo, Q.; Deng, W. Optimal reactive power dispatch using an improved slime mould algorithm. *Energy Rep.* **2021**, *7*, 8742–8759. [[CrossRef](#)]
79. Dai, C.; Chen, W.; Zhu, Y.; Zhang, X. Seeker optimization algorithm for optimal reactive power dispatch. *IEEE Trans. Power Syst.* **2009**, *24*, 1218–1231.
80. Shaw, B.; Mukherjee, V.; Ghoshal, S.P. Solution of reactive power dispatch of power systems by an opposition-based gravitational search algorithm. *Int. J. Electr. Power Energy Syst.* **2014**, *55*, 29–40. [[CrossRef](#)]
81. Elsayed, S.K.; Kamel, S.; Selim, A.; Ahmed, M. An Improved Heap-Based Optimizer for Optimal Reactive Power Dispatch. *IEEE Access* **2021**, *9*, 58319–58336. [[CrossRef](#)]

**Disclaimer/Publisher's Note:** The statements, opinions and data contained in all publications are solely those of the individual author(s) and contributor(s) and not of MDPI and/or the editor(s). MDPI and/or the editor(s) disclaim responsibility for any injury to people or property resulting from any ideas, methods, instructions or products referred to in the content.